NASA/TM-2005-213514

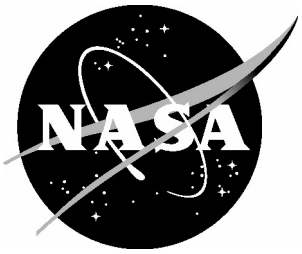

Stalled Pulsing Inertial Oscillation Model for a Tornadic Cyclone

Robert C. Costen
Langley Research Center, Hampton, Virginia

July 2005

The NASA STI Program Office . . . in Profile

Since its founding, NASA has been dedicated to the advancement of aeronautics and space science. The NASA Scientific and Technical Information (STI) Program Office plays a key part in helping NASA maintain this important role.

The NASA STI Program Office is operated by Langley Research Center, the lead center for NASA's scientific and technical information. The NASA STI Program Office provides access to the NASA STI Database, the largest collection of aeronautical and space science STI in the world. The Program Office is also NASA's institutional mechanism for disseminating the results of its research and development activities. These results are published by NASA in the NASA STI Report Series, which includes the following report types:

- TECHNICAL PUBLICATION. Reports of completed research or a major significant phase of research that present the results of NASA programs and include extensive data or theoretical analysis. Includes compilations of significant scientific and technical data and information deemed to be of continuing reference value. NASA counterpart of peer-reviewed formal professional papers, but having less stringent limitations on manuscript length and extent of graphic presentations.

- TECHNICAL MEMORANDUM. Scientific and technical findings that are preliminary or of specialized interest, e.g., quick release reports, working papers, and bibliographies that contain minimal annotation. Does not contain extensive analysis.

- CONTRACTOR REPORT. Scientific and technical findings by NASA-sponsored contractors and grantees.

- CONFERENCE PUBLICATION. Collected papers from scientific and technical conferences, symposia, seminars, or other meetings sponsored or co-sponsored by NASA.

- SPECIAL PUBLICATION. Scientific, technical, or historical information from NASA programs, projects, and missions, often concerned with subjects having substantial public interest.

- TECHNICAL TRANSLATION. English-language translations of foreign scientific and technical material pertinent to NASA's mission.

Specialized services that complement the STI Program Office's diverse offerings include creating custom thesauri, building customized databases, organizing and publishing research results ... even providing videos.

For more information about the NASA STI Program Office, see the following:

- Access the NASA STI Program Home Page at ***http://www.sti.nasa.gov***

- E-mail your question via the Internet to help@sti.nasa.gov

- Fax your question to the NASA STI Help Desk at (301) 621-0134

- Phone the NASA STI Help Desk at (301) 621-0390

- Write to:
  NASA STI Help Desk
  NASA Center for AeroSpace Information
  7121 Standard Drive
  Hanover, MD 21076-1320

NASA/TM-2005-213514

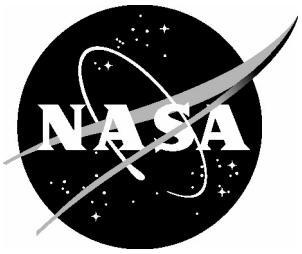

Stalled Pulsing Inertial Oscillation Model for a Tornadic Cyclone

Robert C. Costen
Langley Research Center, Hampton, Virginia

National Aeronautics and
Space Administration

Langley Research Center
Hampton, Virginia 23681-2199

July 2005

Acknowledgments

The author thanks Dr. Joycelyn S. Harrison, Dr. Joanne Simpson, Dennis M. Bushnell, and Harry P. Stough III for their support. He also thanks Susan M. Hurd and Mary L. Edwards for editing the text, Leanna D. Bullock for preparing figures, and Patricia L. Gottschall for desktop publishing.

The use of trademarks or names of manufacturers in the report is for accurate reporting and does not constitute an official endorsement, either expressed or implied, of such products or manufacturers by the National Aeronautics and Space Administration.

Available from:

NASA Center for AeroSpace Information (CASI)
7121 Standard Drive
Hanover, MD 21076-1320
(301) 621-0390

National Technical Information Service (NTIS)
5285 Port Royal Road
Springfield, VA 22161-2171
(703) 605-6000

Abstract

A supercell storm is a tall, rotating thunderstorm that can generate hail and tornadoes. Two models exist for the development of the storm's rotation or mesocyclone—the conventional splitting-storm model, and the more recent pulsing inertial oscillation (PIO) model, in which a nonlinear pulse represents the supercell. Although data support both models and both could operate in the same supercell, neither model has satisfactorily explained the tornadic cyclone. A tornadic cyclone is an elevated vorticity concentration of Rossby number $\mathrm{Ro} \approx 1000$ *that develops within the contracting mesocyclone shortly before a major tornado appears at the surface. We now show that if the internal temperature excess due to latent energy release is limited to the realistic range of –12 K to +12 K, the PIO model can stall part way through the pulse in a state of contraction and spin-up. Should this happen, the stalled-PIO model can evolve into a tornadic cyclone with a central pressure deficit that exceeds 40 mb, which is greater than the largest measured value. This simulation uses data from a major tornadic supercell that occurred over Oklahoma City, Oklahoma, USA, on May 3, 1999. The stalled-PIO mechanism also provides a strategy for human intervention to retard or reverse the development of a tornadic cyclone and its pendant tornado.*

1. Introduction

Supercell storms are tall rotating thunderstorms that can generate hail and tornadoes. Doppler radar images of a hailstorm (Miller, Tuttle, and Knight 1988) show a complex structure that includes an updraft that peaks at midheight, two downdrafts, and a mesocyclone. These features evolve in an environmental flow whose velocity increases and rotates with height. The environmental flow includes a boundary layer at the surface, a highly sheared layer near the storm top, and a midtropospheric layer in which the environmental flow is blocked and must circumnavigate the storm (Brandes 1981). Our modeling study, which is still in a rudimentary state, is limited to the midtropospheric layer and assumes that compatible flows exist in the boundary and upper layers.

Latent energy release drives the vertical flow; however, the source of the rotational flow or mesocyclone is controversial. Two models exist for the generation of the mesocyclone. The first is the conventional splitting-storm model, as reviewed by Doswell (2001), Church et al. (1993), Ray (1986), Klemp (1987), Kessler (1986), Bengtsson and Lighthill (1982), Schlesinger (1980), and others. The second is the pulsing inertial oscillation (PIO) model (Costen and Miller 1998 and Costen and Stock 1992). Data exist that support both the conventional and the PIO models, and both mechanisms could operate in the same supercell.

In the conventional model, a buoyant updraft tilts and stretches horizontal vortex lines in the vertically sheared environmental flow to produce two counterrotating supercells that separate. Such splitting supercell pairs are observed. In fact, we will use data from the cyclonic member of a splitting pair that occurred on May 3, 1999 over Oklahoma City, Oklahoma, USA. However, Davies-Jones (1986) states that observed supercells are predominantly cyclonic. In his modeling studies, Klemp (1987) explains this apparent discrepancy by showing that environmental conditions documented by Maddox (1976) will often weaken or suppress the anticyclonic member of the pair.

Data supplied by Davies-Jones (1986) show that the generation of a major tornado requires a transition wherein the mesocyclone, or a portion thereof, contracts and spins up to a Rossby number $\mathrm{Ro} \approx 1000$, where Ro is the ratio of the vertical spin rate of the cyclone core to the local vertical spin rate of the Earth. This contraction first occurs in the midtropospheric layer, as observed by Doppler radar data presented by Davies-Jones (1986), Vasiloff (1993), and Burgess and Magsig (2000). The contracted mesocyclone is termed a tornadic cyclone because its development aloft precedes the onset of the strongest tornadoes at the surface.

Although the conventional model is well developed, it has not satisfactorily simulated a tornadic cyclone. Modeling studies by Wicker and Wilhelmson (1995) and Wilhelmson and Wicker (2001) produced vorticity concentrations that are strong enough for a tornadic cyclone; however, these concentrations originated at the surface instead of aloft—in conflict with the data. Modeling studies of the flow in a rotating cup by Trapp and Davies-Jones (1997) showed that the height where tornadic vorticity first occurs depends on the vertical distribution of buoyancy; however, it is not clear that their results apply to a free mesocyclone in the troposphere.

The PIO model is in its infancy and does not yet resolve individual updrafts and downdrafts but instead treats the average vertical flow in the core—represented by a uniform time-dependent vertical flow. The model is essentially a Rankine vortex that has been generalized to include the Coriolis force plus this uniform vertical flow within its circular cylindrical core. Ferrel (1889) attributed supercell rotation to the Coriolis force. Scaling studies by Morton (1966), Wallace and Hobbs (1977), Davies-Jones (1986), Holton (1992), and others have since concluded that the Coriolis force is too weak to spin up a supercell storm in the observed time. However, scaling studies rely upon the mechanism, and none of these studies considered the PIO mechanism.

In the compressible continuity and momentum equations used in the PIO model, the vertical temperature lapse of the middle troposphere is neglected and the density is taken to decrease exponentially with height. For our purposes, this approximation is better than the constant density approximation used in the analytic studies of supercell storms by Rotunno and Klemp (1982) and Lilly (1986). However, we will retain the actual temperature lapse in the energy equation and for stability considerations of the midtropospheric layer. Our practice of neglecting terms where they are presumed to be unimportant and retaining them where they are known to be important has precedent elsewhere in Atmospheric Science, for example, in the Boussinesq approximation (Menke and Abbott 1990), which we do not use.

In our postulated environment, rising parcels of air expand (dilatate) and descending parcels contract. The key approximation used in the PIO and stalled-PIO models is that the horizontal divergence in the core results predominantly from this three-dimensional dilatation; that is, the horizontal divergence is approximately equal to the speed of the vertical flow divided by the scale height. We shall refer to this approximation as the "dilatation-horizontal divergence" approximation or simply the "DHD" approximation. It follows that when the vertical flow in the core is downward, the cylindrical core contracts. This contraction causes the core to spin up, partly by increasing the concentration of existing vertical vorticity and partly by the action of the Coriolis force on the convergent flow. Likewise, upward flow causes the core to expand and spin down. This feature of spin-up occurring in a downdraft is in contrast to the conventional splitting-storm model, where spin-up occurs in an updraft.

Various arguments can be advanced to support the DHD approximation, as in the statement that follows equation (2.4); however, it seems clearest simply to test the accuracy of the DHD approximation during the model runs, and this we will do. The DHD approximation neglects certain terms in the continuity equation. We will compute both the retained terms and the neglected terms and will show by plotting their ratio that the DHD approximation is reasonably accurate during our model runs.

In the PIO model, the generalized Rankine vortex contracts, expands, and translates in the midtropospheric layer in accordance with a nonlinear inertial oscillation, whose period is typically about 19 hr. The pulse phase of this oscillation, which coincides with the contracted state of the vortex, is identified with a single cyclonic or anticyclonic supercell.

According to data presented by Costen and Miller (1998), only the pulse phase of the PIO model is actually observed in the troposphere; that is, the oscillation starts at the beginning of a pulse, proceeds through the pulse (supercell storm), and terminates shortly afterwards. Therefore, we will limit our present simulations to the pulse phase. For simulations of the complete period, see Costen and Miller (1998) and Costen and Stock (1992).

Because of the DHD approximation and the prescribed vertical dependence of density, the continuity and momentum equations are sufficient to obtain the PIO and stalled-PIO solutions for the vorticity, horizontal divergence, velocity, pressure, core radius, core buoyancy, mesocyclonic circulation, and cloud base mass influx. The equation of state for a dry, perfect gas then determines the temperature, which, as mentioned, turns out to be isothermal, except for a uniform temperature excess or deficit in the core. The energy equation serves only to determine the thermal input power or latent energy release that is required to support the PIO and stalled-PIO solutions.

Although the PIO is driven by latent energy release, the oscillation is controlled by horizontal inertial flow (Haltiner and Martin 1957 and Holton 1992) that is organized into a radial oscillation. When viewed from above (fig. 1(a)), every parcel on the periphery of the contracting core traverses an anticyclonic circular arc such that the parcel's centrifugal force balances the Coriolis force and the horizontal pressure gradient is zero. Costen and Stock (1992) show that the same is true for every parcel inside the core. Consequently, the PIO model has no central pressure deficit (prior to a stall). During contraction, each parcel in the core is compressed by descending in a uniform downdraft. When the core reaches its minimum radius and maximum spin-up, the downdraft ceases. The subsequent inertial trajectories (fig. 1(b)) cause the core to expand and spin down, which requires an upward flow in the core.

Compared with the complicated structure of a supercell described earlier, the PIO model, in its present state of development, is a zeroth-order approximation. The vertical speed, horizontal divergence, vorticity, and buoyancy—all of which are uniform in the core of the PIO model—are zeroth-order approximations to the instantaneous spatial average values of these fields in the core of an actual supercell. The vertical flow reversal (described in the previous paragraph) that occurs at the midpoint of the pulse in the PIO model therefore represents a reversal in the *average* vertical flow of an actual supercell.

The PIO model determines the amount of core buoyancy required to sustain the oscillation. The average downdraft that occurs during spin-up at the onset of a pulse requires a moderate amount of negative buoyancy that results from evaporative cooling of midtropospheric moisture. However, the average draft reversal that occurs at the midpoint of the pulse requires a large spike of positive buoyancy. This spike is generated by condensational heating of moist surface air that is lifted in a convectively unstable environment by the gust front of the downdraft.

Costen and Miller (1998) showed that the available buoyancy range limits the maximum Rossby number that the PIO can achieve. We define the available buoyancy by a core temperature excess ΔT in the range $(-12\ \mathrm{K} \le \Delta T \le 12\ \mathrm{K})$, as suggested by sounding data presented by Miller, Tuttle, and Knight (1988). The PIO solution then gives a maximum Rossby number of $\mathrm{Ro} \approx 100$, which is an order of magnitude too low for a tornadic cyclone. However, we will now show that this same available buoyancy range can cause the PIO model to stall in a state of contraction and spin-up. Our objective is to model the

flow after such a stall has occurred and to demonstrate that it can produce a tornadic cyclone. Since the PIO and stalled-PIO models apply in the midtropospheric layer, the resultant tornadic cyclone develops aloft, in agreement with observation.

A remarkable feature of the PIO model is that its track over the surface of the Earth during the pulse phase resembles the dogleg track of an actual supercell hailstorm, as shown by Costen and Miller (1998) and Costen and Stock (1992). After a stall has occurred, however, the track equations disappear from the model, so we will not attempt any track simulations here. The issue of the post-stall track must await further research.

As mentioned, the PIO and stalled-PIO models will use data from the May 3, 1999 supercell storm that occurred over greater Oklahoma City, Oklahoma. This supercell (Supercell A) was the right-hand member of a splitting supercell pair. It generated a 1.6-km-wide tornado (Tornado A9) that killed 36 people and injured 583. This tornado also inflicted property damage of 1 billion United States dollars (USD) along its 60-km track. Rated F5 (maximum intensity) on the Fujita scale (Fujita 1973), the tornado possibly reached wind speeds of 318 mph, as indicated by preliminary Doppler radar data. Burgess and Magsig (2000) present time-height data that confirm that an elevated tornadic cyclone developed in Supercell A about 5 min before the start of Tornado A9, that this tornadic cyclone persisted with some variation throughout the 80-min lifetime of Tornado A9, and that the tornadic cyclone dissipated about 3 min before this tornado ended.

Although we use data from Supercell A, we will not attempt a precise simulation of this storm. Instead we will explore the capabilities of the PIO and stalled-PIO models within the framework of these data. While awaiting publication of a value for the mesocyclonic circulation of Supercell A, we have used a typical value given by Davies-Jones (1986) of $\Gamma_{\max} = 5 \times 10^5$ m^2 s^{-1}. We will always initialize the core radius such that this value for circulation is achieved at the time of maximum contraction and spin-up. As mentioned, the model computes the thermal input power $Q(t)$ from latent energy release and the mass influx at cloud base $M(t)$. While also awaiting these values from Supercell A, we have compared our computed values with measured reference values of $Q_{\text{ref}} = 1.9 \times 10^{13}$ W and $M_{\text{ref}} = 1.2 \times 10^9$ kg s^{-1} presented by Foote and Fankhauser (1973) for a different supercell.

Sections 2 to 4 give a review of the PIO model and point up a naturally occurring condition that could cause the model to stall in a state of contraction and spin-up. Sections 5 and 6 give the mathematics of tornadic cyclone development after such a stall has occurred. In section 7, the stalled-PIO model is applied to Tornadic Cyclone A9, with some attention given to the possibility of human intervention to promote early termination. Concluding remarks are presented in section 8.

2. Relevant Aspects of PIO Model

2.1. Tangential Coordinate Frame

The model uses the local tangential Cartesian frame shown in figure 2. The origin is fixed at mean sea level (MSL) on the Earth's surface, and the x, y, and z axes point eastward, northward, and upward, respectively. (Cylindrical coordinates r, θ, and z are also used, where $x = r\cos\theta$ and $y = r\sin\theta$.) Although the x and y axes do not curve with the Earth's surface, Haltiner and Martin (1957) show that this frame is adequate for describing tropospheric flows within a horizontal radius of about 60 km. This radius is sufficient to contain the convective core of a supercell, but not all the outer flow. In this frame,

the fluid velocity is denoted by $\mathbf{v} = (u, v, w)$ (m s^{-1}), the vorticity by $\boldsymbol{\omega} = \mathrm{curl}\mathbf{v} = (\xi, \eta, \zeta)$ (s^{-1}), the divergence by $D = \mathrm{div}\mathbf{v} = \partial u/\partial x + \partial v/\partial y + \partial w/\partial z$ (s^{-1}), and the angular velocity of the Earth by $\boldsymbol{\Omega} = (0, \Omega_y, \Omega_z)$ (rad s^{-1}). The components Ω_y and Ω_z, although slowly varying functions of y, are treated as constants, which is reasonable for the horizontal radius given previously.

2.2. Generalized Rankine Vortex

The generalized Rankine vortex shown in figure 2 is intended to represent the convective core of a supercell storm that upon further contraction and spin-up can become a tornadic cyclone. The core radius is $a(t)$. The centerline is located at $[x_c(t), y_c(t)]$. The vertical vorticity $\zeta(t)$ is uniform inside the core $[r < a(t)]$ and zero in the outer region $[r > a(t)]$. The midtropospheric layer, which is between the planetary boundary layer below and the highly sheared layer above, is given by $(b \le z \le h)$. The density ρ (kg m^{-3}) is taken to decrease exponentially with height z. This stipulation neglects the temperature lapse between b and h. Rising/falling parcels of air dilatate and contribute to the divergence $D(t)$, which is also taken to be uniform inside the core and zero in the outer region. The core fluid is uniformly buoyant, with a normalized density deficit $B(t)$, which is called simply the buoyancy. Lateral entrainment, friction, and heat conduction are neglected, which is reasonable for a supercell storm in the midtropospheric layer.

The density of the outer fluid at radius a is given by

$$\rho^0(a, z) = \rho_b^0 \, \mathrm{e}^{-\varepsilon Z} \tag{2.1}$$

where the fields in the outer region are distinguished by the superscript 0 and $Z \equiv z - b$. The coefficient ρ_b^0 and the inverse density scale height ε (in m^{-1}) are constants. Inside the core, the density is given by

$$\rho(z, t) = \rho_b^0 [1 - B(t)] \mathrm{e}^{-\varepsilon Z} \tag{2.2}$$

The buoyancy $B(t) << 1$, because it corresponds to a temperature excess or deficit of at most 12 K, as mentioned, and terms of $O(B^2)$ will always be neglected.

The continuity equation is given by

$$\frac{\partial \rho}{\partial t} + \mathbf{v} \cdot \nabla \rho + \rho D = 0 \tag{2.3}$$

Substituting the inner density (eq. (2.2)) in equation (2.3) and dividing by ρ gives

$$-\dot{B} - \varepsilon w + D = 0 \tag{2.4}$$

where an overhead dot denotes an ordinary time derivative. Retaining the effects of $B(t)$ on the buoyant force but neglecting its effects on $D(t)$, we have

$$D(t) = \varepsilon w(t) \tag{2.5}$$

which is the key approximation used in both the PIO and stalled-PIO models, wherein D and εw will be used interchangeably. Equation (2.5) confirms that the vertical component of velocity $w(t)$ is also spatially uniform inside the core so that $D(t)$ is purely horizontal divergence given by

$$D(t) = \frac{\partial u}{\partial x} + \frac{\partial v}{\partial y} \tag{2.6}$$

Hence, approximation (eq. (2.5)) states that the horizontal divergence inside the core results predominantly from the dilatation of ascending/descending air parcels. We call equation (2.5) the "dilatation-horizontal divergence" approximation, or simply the "DHD" approximation. To check the accuracy of this approximation, we will plot the ratio $R_{\text{DHD approx}}$ of neglected to retained terms in equation (2.3); for the PIO model this ratio is given from equation (2.4) by

$$R^{\text{PIO}}_{\text{DHD approx}} = \left| \frac{\dot{B}}{D} \right| \tag{2.7}$$

Also included in the core is a horizontal flow with vertical wind shear that is represented by the constants U_b and V_b and the horizontal vorticity components $\xi(t)$ and $\eta(t)$.

3. Inner Reduction

3.1. Velocity Field

The complete velocity field inside the core is given by

$$u(x,y,z,t) = U_b + \eta(t)Z + \frac{1}{2}[D(t)X(x,t) - \zeta(t)Y(y,t)] \tag{3.1a}$$

$$v(x,y,z,t) = V_b - \xi(t)Z + \frac{1}{2}[D(t)Y(y,t) + \zeta(t)X(x,t)] \tag{3.1b}$$

$$w(x,y,z,t) = w(t) = \frac{D(t)}{\varepsilon} \tag{3.1c}$$

where $X(x,t) \equiv x - x_c(t)$ and $Y(y,t) \equiv y - y_c(t)$. The constants U_b and V_b represent the stationary part of the horizontal flow inside the core, and $\eta(t)Z$ and $-\xi(t)Z$ represent the inner vertical wind shear. The terms $-\zeta(t)Y/2$ and $\zeta(t)X/2$ represent the inner flow of the Rankine vortex. The angular velocity of the core fluid $\dot{\theta}$ (in rad s^{-1}) and the Rossby number Ro are given by

$$\dot{\theta} = \frac{\zeta}{2} \qquad \text{Ro} = \frac{\zeta}{2\Omega_z} \tag{3.2}$$

The terms $D(t)X/2$ and $D(t)Y/2$ represent the inner radial horizontal flow that results from the horizontal divergence.

3.2. Momentum Equation

The inviscid, compressible momentum equation is given by

$$\frac{\partial \mathbf{v}}{\partial t} + \boldsymbol{\omega} \times \mathbf{v} + \nabla \frac{v^2}{2} + \frac{\nabla p}{\rho} + \nabla \Phi + 2\boldsymbol{\Omega} \times \mathbf{v} = 0 \tag{3.3}$$

where v^2 is $\mathbf{v} \cdot \mathbf{v}$, p is the pressure (Pa), Φ is the geopotential gz ($m^2\ s^{-2}$), and g is the gravitational acceleration (9.81 $m\ s^{-2}$).

Solving equation (3.3) for ∇p and substituting the inner velocity field (eqs. (3.1)), we find

$$\frac{\partial p}{\partial x} = -\frac{\rho}{2}\left(G_1 - G_3 v + Du\right) \tag{3.4a}$$

$$\frac{\partial p}{\partial y} = -\frac{\rho}{2}\left(G_2 + G_3 u + Dv\right) \tag{3.4b}$$

$$\frac{\partial p}{\partial z} = -\rho\left(g + \frac{\dot{D}}{\varepsilon} - 2\Omega_y u\right) \tag{3.4c}$$

where

$$G_1 \equiv \dot{D}X - \dot{\zeta}\ Y - D\dot{x}_c + \zeta\ \dot{y}_c + 2\dot{\eta}Z + 2\frac{D}{\varepsilon}\left(\eta + 2\Omega_y\right) \tag{3.5a}$$

$$G_2 \equiv \dot{D}Y + \dot{\zeta}\ X - \zeta\ \dot{x}_c - D\dot{y}_c - 2\dot{\xi}Z - 2\frac{D}{\varepsilon}\xi \tag{3.5b}$$

$$G_3 \equiv \zeta + 4\Omega_z \tag{3.5c}$$

3.3. Second-Order Partial Derivatives and Nonlinear Harmonic Equations

In the midtropospheric layer, we assume that p and its first- and second-order partial derivatives are continuous functions of $x, y,$ and z (except at radius a, where p must be continuous but its derivatives could be discontinuous). It follows for $(r < a,\ b \le z \le h)$ that

$$\frac{\partial^2 p}{\partial x\ \partial y} = \frac{\partial^2 p}{\partial y\ \partial x} \qquad \frac{\partial^2 p}{\partial x\ \partial z} = \frac{\partial^2 p}{\partial z\ \partial x} \qquad \frac{\partial^2 p}{\partial y\ \partial z} = \frac{\partial^2 p}{\partial z\ \partial y} \tag{3.6}$$

Substituting the cross derivatives of equations (3.4) in equations (3.6), dividing by ρ, and setting the coefficients of X, Y, and Z individually to zero in each equation, we obtain the following set of coupled ordinary differential equations (ODEs):

$$\dot{\xi} = \frac{1}{2}\left[\eta\left(\zeta + 4\Omega_z\right) - D\xi\right] \tag{3.7a}$$

$$\dot{\eta} = -\frac{1}{2}\left[\xi\left(\zeta + 4\Omega_z\right) + D\eta\right] \tag{3.7b}$$

$$\dot{\zeta} = -D\left(\zeta + 2\Omega_z\right) \tag{3.7c}$$

$$\dot{D} = \frac{1}{2}\left[\zeta\left(\zeta + 4\Omega_z\right) - D^2\right] \tag{3.8}$$

$$\dot{x}_c = U_b + \frac{2}{\varepsilon}\Omega_y + \frac{2}{\zeta^2 + D^2}\left[\zeta\left(-\xi w + 2\Omega_z U_b\right) + D\left(\eta w - 2\Omega_z V_b\right)\right] \tag{3.9a}$$

$$\dot{y}_c = V_b + \frac{2}{\zeta^2 + D^2}\left[\zeta\left(-\eta w + 2\Omega_z V_b\right) + D\left(-\xi w + 2\Omega_z U_b\right)\right] \tag{3.9b}$$

3.4. Pressure Field

To obtain the inner pressure field p, we first substitute equations (3.7), (3.8), (3.9), and (2.2) into the pressure gradient (eqs. (3.4)), which gives

$$\frac{\partial p}{\partial x} = -\rho_b^0 e^{-\varepsilon Z}(1 - B)\,\Omega_y \frac{D}{\varepsilon} \tag{3.10a}$$

$$\frac{\partial p}{\partial y} = \rho_b^0 e^{-\varepsilon Z}(1 - B)\,\Omega_y \frac{\zeta}{\varepsilon} \tag{3.10b}$$

$$\frac{\partial p}{\partial z} = -\rho_b^0 e^{-\varepsilon Z}(1 - B)\left\{g + \dot{w} - 2\Omega_y\left[U_b + \eta Z + \frac{1}{2}(DX - \zeta\, Y)\right]\right\} \tag{3.10c}$$

These partial derivatives can now be integrated to obtain p as

$$p(x, y, z, t) = \rho_b^0 e^{-\varepsilon Z}(1 - B)\frac{g}{\varepsilon}\left\{1 + \frac{\dot{w}}{g} - \frac{2\Omega_y}{g}\left[\frac{\eta}{\varepsilon} + U_b + \eta Z + \frac{1}{2}(DX - \zeta\, Y)\right]\right\} \tag{3.11}$$

This result confirms that the PIO model has no pressure deficit at its center, where $X = Y = 0$, which is consistent with inertial flow. According to Davies-Jones (1986), the pressure deficit in mesocyclones is typically about 5 mb, although it has been measured as high as 34 mb. This discrepancy indicates the occurrence of a partial transition from inertial flow to cyclostrophic flow, where the centrifugal force on parcels is balanced by the radial pressure gradient, as discussed in sections 5 and 6.

Thus far, we have reduced the inner solution to a time-dependent set of ODEs, except that we have no equations for $a(t)$ or $B(t)$. These quantities are determined by the jump conditions at the cylindrical interface between the inner and outer solutions, as shown in figure 2. Instead of attempting a nonsymmetric, translating outer solution, we will revert to an axisymmetric, nontranslating solution that is sufficient for obtaining $a(t)$ and $B(t)$. We assume that the results so obtained apply approximately to the

translating model. This assumption will fail if the inner flow of the translating model does not block the relative environmental wind, which will then erode the core.

4. Axisymmetric, Nontranslating PIO Model

4.1. Inner Solution

For the PIO model to remain centered on the origin (i.e., for $\dot{x}_c = \dot{y}_c = 0$), we must take $U_b = V_b = \xi = \eta = \Omega_y = 0$. The velocity (eqs. (3.1)) and pressure (eq. (3.11)) then become, in cylindrical coordinates,

$$v_r(r,t) = \frac{D(t)}{2} r \tag{4.1a}$$

$$v_\theta(r,t) = \frac{\zeta(t)}{2} r \tag{4.1b}$$

$$v_z(t) = w(t) = \frac{D(t)}{\varepsilon} \tag{4.1c}$$

$$p(z,t) = \rho_b^0 e^{-\varepsilon Z} \frac{g}{\varepsilon}\left[1 - B(t)\right]\left[1 + \frac{\dot{w}(t)}{g}\right] \tag{4.2}$$

4.2. Outer Solution

Because the external vorticity $\boldsymbol{\omega}^0$ and divergence D^0 are zero, the outer velocity field is given by (for $r \geq a$)

$$v_r^0(r,t) = \frac{D(t)a^2(t)}{2r} \tag{4.3a}$$

$$v_\theta^0(r,t) = \frac{\zeta(t)a^2(t)}{2r} \tag{4.3b}$$

$$v_z^0 = w^0 = 0 \tag{4.3c}$$

The field v_r is continuous at the interface $r = a(t)$, as required by the jump conditions for the continuity and momentum equations. The field v_θ is also continuous, but w, ρ, D, and ζ all have finite discontinuities. The requirement that the interface moves with the fluid gives the desired equation for core radius

$$\dot{a} = \frac{Da}{2} \tag{4.4}$$

The core buoyancy $B(t)$ can be determined from the jump condition that the pressure is continuous at $r = a$. To determine the outer pressure field, we first solve the momentum equation (3.3) for the pressure gradient in cylindrical coordinates and then substitute the outer velocity field (eqs. (4.3)) and the tendencies (eqs. (3.7c), (3.8), and (4.4)) to obtain

$$\frac{\partial p^0}{\partial r} = -\frac{gF\rho^0}{\varepsilon r}\left(1 - \frac{a^2}{r^2}\right) \tag{4.5a}$$

$$\frac{\partial p^0}{\partial \theta} = 0 \tag{4.5b}$$

$$\frac{\partial p^0}{\partial z} = -g\rho^0 \tag{4.5c}$$

where F, the Froude number, is a constant of the motion given by

$$F = \frac{\varepsilon a^2}{4g}\left(\zeta^2 + D^2\right) \tag{4.6}$$

Its constancy for the PIO model is demonstrated by taking its time derivative and substituting the tendencies (eqs. (3.7c), (3.8), and (4.4)).

As with the inner solution, we require

$$\frac{\partial^2 p^0}{\partial r\ \partial z} = \frac{\partial^2 p^0}{\partial z\ \partial r} \qquad (r > a,\ b \le z \le h) \tag{4.7}$$

Consequently, the outer density ρ^0 must satisfy

$$\frac{\partial \rho^0}{\partial r} = \frac{F}{\varepsilon r}\left(1 - \frac{a^2}{r^2}\right)\frac{\partial \rho^0}{\partial z} \tag{4.8}$$

The solution of this equation that satisfies the boundary condition (eq. (2.1)) at $r = a$ is given by

$$\rho^0(r,z,t) = \rho_b^0\left(\frac{a}{r}\right)^F \exp\left[-\varepsilon Z + \frac{F}{2}\left(1 - \frac{a^2}{r^2}\right)\right] \tag{4.9}$$

Substituting this result in equations (4.5) and integrating for the outer pressure, we obtain the hydrostatic result

$$p^0(r,z,t) = \frac{g}{\varepsilon}\rho^0(r,z,t) = \rho_b^0\frac{g}{\varepsilon}\left(\frac{a}{r}\right)^F \exp\left[-\varepsilon Z + \frac{F}{2}\left(1 - \frac{a^2}{r^2}\right)\right] \tag{4.10}$$

Both $p^0(r,z,t)$ and $\rho^0(r,z,t)$ have their maximum values at $r = a$ and approach zero as $r \to \infty$, which is reasonable for our tangential coordinate frame. To conform with the notation for the stalled-PIO model that will be developed in sections 5 and 6, we associate the maximum external pressure $p^0(a,b)$ and density $\rho^0(a,b)$ at height b with the environmental pressure p_b^{envir} and density ρ_b^{envir} at height b, which are constants. Then, by equation (4.10), we have

$$\rho_b^0 = \rho_b^{\text{envir}} = \frac{\varepsilon}{g} p_b^{\text{envir}} \tag{4.11}$$

and the expressions for the outer pressure (eq. (4.10)), inner pressure (eq. (4.2)), and inner density (eq. (2.2)) become

$$p^0(r,z,t) = \frac{g}{\varepsilon}\rho^0(r,z,t) = p_b^{\text{envir}} \left(\frac{a}{r}\right)^F \exp\left[-\varepsilon Z + \frac{F}{2}\left(1 - \frac{a^2}{r^2}\right)\right] \tag{4.12}$$

$$p(z,t) = p_b^{\text{envir}} e^{-\varepsilon Z}\left[1 - B(t)\right]\left[1 + \frac{\dot{w}(t)}{g}\right] \tag{4.13}$$

$$\rho(z,t) = \frac{\varepsilon}{g} p_b^{\text{envir}} (1 - B)\, e^{-eZ} \tag{4.14}$$

4.3. Buoyancy and Inner Pressure

By equating the outer pressure (eq. (4.12)) and the inner pressure (eq. (4.13)) at $r = a$, we obtain the desired equation for buoyancy

$$B(t) = \frac{\dot{w}(t)}{g} \tag{4.15}$$

This expression is similar to that given by Darkow (1986) for the vertical acceleration of a nonentraining buoyant parcel. The inner pressure is now independent of t and is given by

$$p(z) = p_b^{\text{envir}} e^{-\varepsilon Z} \tag{4.16}$$

By equation (3.8), the buoyancy (eq. (4.15)) for the PIO can also be determined from the formula

$$B^{\text{PIO}} = \frac{1}{2\varepsilon g}\left[\zeta\left(\zeta + 4\Omega_z\right) - D^2\right] \tag{4.17}$$

4.4. Supplementary Formulas

The mesocyclonic circulation Γ is given by (in $m^2\ s^{-1}$)

$$\Gamma = \pi a^2 \zeta \tag{4.18}$$

and the cloud base mass influx M by (in kg s^{-1})

$$M = 2\pi w \int_0^a r\rho(r,b,t)\,\mathrm{d}r \tag{4.19}$$

Substitution of equation (4.14) gives for the PIO

$$M^{\mathrm{PIO}} = \frac{\pi}{g} a^2 D(1-B) p_b^{\mathrm{envir}} \tag{4.20}$$

The temperature is determined from the equation of state for a dry perfect gas

$$p = \rho R T \tag{4.21}$$

which we apply to both the inner and outer regions, where R, the gas constant, equals 287 J kg^{-1} K^{-1}. As mentioned, the outer temperature T^0 in the model is a constant

$$T^0 = \frac{g}{\varepsilon R} \tag{4.22}$$

In practice, this formula determines the inverse scale height ε from a measurement of T^0, which we will take to be the environmental temperature at height b. The inner temperature T is given by

$$T(t) = T^0\left[1 + B(t)\right] \tag{4.23}$$

Thus, the model core is also isothermal, but its temperature varies with the buoyancy. Solving equation (4.23) for B, we confirm that

$$B(t) = \frac{T(t) - T^0}{T^0} \equiv \frac{\Delta T(t)}{T^0} \tag{4.24}$$

The energy equation for a dry perfect gas, as given by Holton (1992), can be written

$$q = \rho c_p \left(\frac{\partial}{\partial t} + \mathbf{v}\cdot\nabla\right) T - \left(\frac{\partial}{\partial t} + \mathbf{v}\cdot\nabla\right) p \tag{4.25}$$

where q (in W m^{-3}) is the diabatic heating rate, which is usually due to latent energy release, and c_p equals 1004 J kg^{-1} K^{-1}. Substituting the inner pressure (eq. (4.16)) and temperature (eq. (4.23)) and integrating over the core volume, we obtain the total thermal input power Q (in W) required to support the PIO

$$Q^{\mathrm{PIO}} = p_b^{\mathrm{envir}} \frac{\pi a^2}{\varepsilon}\left[\frac{\varepsilon}{g} c_p T^0 \dot{B} + D\left(\frac{c_p}{g}\frac{\mathrm{d}T^0}{\mathrm{d}z} + 1\right)\right]\left[1 - \mathrm{e}^{-\varepsilon(h-b)}\right] \tag{4.26}$$

As explained, although we have neglected the temperature lapse $\mathrm{d}T^0/\mathrm{d}z$ in the continuity and momentum equations, we have retained it here to be more accurate when applying this formula to an actual supercell. The corresponding water vapor influx M_v (in kg s^{-1}) is given by

$$M_v = \frac{Q}{L_c} \tag{4.27}$$

where L_c, the latent heat of condensation, equals 2.5×10^6 J kg^{-1}.

4.5. Maximal PIO Plots

Plots of ΔT, w, a, Ro, $R_{\mathrm{DHD\ approx}}$, Γ, M, and Q versus t are shown in figure 3 for a 2-hr interval centered on the pulse phase of the PIO. The corresponding inertial trajectories of parcels on the core periphery were previously shown in figure 1(b). Although equations (3.7c) and (3.8) have an analytic solution (Costen and Miller 1998), these two equations and equations (4.4) were integrated numerically by using a fourth-order Runge-Kutta routine. The relevant parameters, listed in table 1, are taken from data on Supercell A that was provided by Edwards and Thompson (2000) and Burgess and Magsig (2000). The initial values listed in table 2 were chosen so that the mesocyclonic circulation at maximum contraction and spin-up has the value $\Gamma_{\max} = 5 \times 10^5$ m^2 s^{-1} and the core temperature excess ΔT plotted in figure 3(a) just stays within the available range $(-12\ \mathrm{K} \le \Delta T \le 12\ \mathrm{K})$, which corresponds to buoyancy $B(t)$ in the range $(-0.04158 \le B(t) \le 0.04158)$.

As shown in figure 3(a), ΔT peaks at +12 K, which corresponds to the maximal PIO. The corresponding core buoyancy drives the vertical speed w shown in figure 3(b). By the DHD approximation (eq. (2.5)), the horizontal divergence D is proportional to w, so the core radius a varies as shown in figure 3(c). The resulting peak Rossby number, as shown in figure 3(d), is the largest the PIO mechanism can produce for the environment of Supercell A. As mentioned, this value $\mathrm{Ro} = 118.5$ is an order of magnitude less than that required for Tornadic Cyclone A9. Figure 3(e) is a plot of the ratio $R_{\mathrm{DHD\ approx}}$, as given by equation (2.7), and shows that this ratio is very small except for a brief interval in the middle of the pulse when it reaches 0.12 as both $\dot{B}$ and D pass through zero. We conclude that the DHD approximation was reasonably accurate during this PIO model run.

The mesocyclonic circulation Γ, as shown in figure 3(f), starts out anticyclonic, achieves the targeted cyclonic peak value of $\Gamma_{\max} = 5 \times 10^5$ m^2 s^{-1}, and eventually becomes anticyclonic again, in agreement with the inertial trajectories shown in figure 1(b). The cloud base mass influx M from equation (4.20) is shown in figure 3(g) and the thermal input power Q from (4.26) in figure 3(h). The perturbation in Q at $t \approx 60$ min results from the $\dot{B}$ term; otherwise, Q is negative during the downdraft phase and positive during the updraft phase because downdrafts generally require evaporative cooling and thus are exothermic, while updrafts require condensational heating and are endothermic.

A comparison of figures 3(a)–(d) confirms that spin-up occurs in a contracting cylindrical downdraft that is driven by moderate negative buoyancy. At the midpoint of the pulse, the contracting downdraft reverses and becomes an expanding updraft that causes the mesocyclone to spin down. This rapid draft reversal requires a large spike of positive buoyancy.

4.6. Condition for PIO To Stall

Figure 3(a) depicts an 8 to 1 asymmetry between the +12 K and −1.5 K excursions of the core temperature excess ΔT. Since the negative value of ΔT occurs first, we are free to initialize the PIO model, as shown in table 3, so that ΔT decreases to a minimum value of −12 K. The subsequent maximum value of +96 K is far outside the given available range of ($-12\ \text{K} \le \Delta T \le 12\ \text{K}$). We infer that upon reaching $\Delta T = +12\ \text{K}$, the PIO model would stall, as shown in figure 4(a). Our task now is to develop a model that applies after such a stall has occurred.

The physical mechanism shown in figures 1 and 3 gives insights about what should happen after a stall. The truncated positive buoyancy shown in figure 4(a) is insufficient to cause the rapid draft reversal required for the core to expand in accordance with the inertial trajectories shown in figure 1(b). Consequently, the parcels would become trapped in orbits about the contracted cyclone center. Since the Coriolis force could no longer balance the centrifugal force, depressions in the pressure and density would begin to develop at the center, and the flow would undergo a transition from inertial to cyclostrophic.

5. Stalled-PIO Solution

To allow for the development of such depressions in pressure and density after the stall, we must generalize the outer and inner densities as follows. At the interface $r = a$, we now take

$$\rho^0(a,z,t) = \sigma_b^0(t)\mathrm{e}^{-\varepsilon Z} \tag{5.1}$$

$$\rho(a,z,t) = \sigma_b^0(t)\left[1 - B(t)\right]\mathrm{e}^{-\varepsilon Z} \tag{5.2}$$

and for the inner density

$$\rho(x,y,z,t) = \sigma(X,Y,Z,t)\left[1 - B(t)\right]\mathrm{e}^{-\varepsilon Z} \tag{5.3}$$

where $B(t)$ is now a $given$ function of t that is confined to the available range ($-0.04158 \le B(t) \le 0.04158$), which corresponds to ($-12\text{K} \le \Delta T(t) \le 12\ \text{K}$). Although the inner analysis will use $\sigma(X,Y,Z,t)$ to establish certain generalities, the model runs will revert to a simplified axisymmetric $\sigma(r,t)$. Substituting this simplified inner density into the continuity equation (2.3) gives

$$\frac{1}{\sigma}\left(\frac{\partial\sigma}{\partial t} + v_r\frac{\partial\sigma}{\partial r}\right) - \dot{B} - \varepsilon w + D = 0 \tag{5.4}$$

As mentioned, we will retain the DHD approximation (eq. (2.5)) after the stall, and we will continue to plot the ratio $R_{\text{DHD approx}}$ of neglected to retained terms by using the formula

$$R_{\text{DHD approx}}^{\text{stalled PIO}} = \left|\frac{1}{D}\left[\dot{B} - \left(\frac{\partial}{\partial t} + v_r\frac{\partial}{\partial r}\right)\ln\sigma\right]\right| \tag{5.5}$$

The same idealized inner velocity fields (eqs. (3.1)) are used in the analysis after the stall, and the momentum equation (3.3) can be written

$$-2\nabla p = \rho\mathbf{A} \tag{5.6}$$

where

$$A_1 \equiv G_1 - G_3 v + Du \tag{5.7a}$$

$$A_2 \equiv G_2 + G_3 u + Dv \tag{5.7b}$$

$$A_3 \equiv 2g + \frac{2}{\varepsilon}\dot{D} - 4\Omega_y u \tag{5.7c}$$

and **G** is given by equations (3.5). Substituting the density (eq. (5.3)) into equation (5.6), enforcing the cross-derivative equations (3.6), and defining

$$L \equiv \ln\sigma - \varepsilon Z \tag{5.8}$$

we obtain

$$\mathbf{A} \times \nabla L = \mathrm{curl}\mathbf{A} \tag{5.9}$$

By equation (5.6), we have

$$\mathrm{curl}\mathbf{A} = -2\nabla\left(\frac{1}{\rho}\right) \times \nabla p \tag{5.10}$$

Although the flow at the interface $r = a$ is baroclinic because of the jump in density, we take the inner flow to be barotropic so that

$$\mathrm{curl}\mathbf{A} = 0 \qquad (r < a) \tag{5.11}$$

and

$$\mathbf{A} \times \nabla L = 0 \qquad (r < a) \tag{5.12}$$

If equations (5.7), (3.5), and (3.1) are substituted into equation (5.11), we obtain

$$\dot{\xi} = \frac{1}{2}\left[\eta\left(\zeta + 4\Omega_z\right) - D\xi\right] - \Omega_y \zeta \tag{5.13a}$$

$$\dot{\eta} = -\frac{1}{2}\left[\xi\left(\zeta + 4\Omega_z\right) + D\eta\right] - \Omega_y D \tag{5.13b}$$

$$\dot{\zeta} = -D\left(\zeta + 2\Omega_z\right) \tag{5.13c}$$

The expression (eq. (5.13c)) for $\dot{\zeta}$ is identical to equation (3.7c) for the PIO. Except for the Ω_y terms, equations (5.13a) and (5.13b) for $\dot{\xi}$ and $\dot{\eta}$ are the same as equations (3.7a) and (3.7b) for the PIO. However, after a stall, there are no equations for $\dot{D}$, $\dot{x}_c$, or $\dot{y}_c$ that are comparable to equations (3.8),

(3.9a), and (3.9b) for the PIO. The absence of the $\dot{D}$ equation is fortunate because we now need $\dot{D}$ to be determined solely by the prescribed buoyancy $B(t)$. The absence of equations for $\dot{x}_c$ and $\dot{y}_c$ means that the inner pressure can be determined for any given values of $\dot{x}_c$ and $\dot{y}_c$; that is, the track after a stall is not determined by our midtropospheric model as it was before the stall had occurred.

When results (eqs. (5.13)) are substituted back into equation (5.7), we obtain

$$A_1 = \alpha X - 2\Omega_y D\left(Z - \frac{2}{\varepsilon}\right) - D\left(\dot{x}_c - U_b\right) + \zeta\left(\dot{y}_c - V_b\right) + \frac{2D}{\varepsilon}\eta - 4\Omega_z V_b \tag{5.14a}$$

$$A_2 = \alpha Y + 2\Omega_y \zeta Z - \zeta\left(\dot{x}_c - U_b\right) - D\left(\dot{y}_c - V_b\right) - \frac{2D}{\varepsilon}\xi + 4\Omega_z U_b \tag{5.14b}$$

$$A_3 = 2\left(g + \frac{\dot{D}}{\varepsilon}\right) - 4\Omega_y\left[U_b + \eta Z + \frac{1}{2}\left(DX - \zeta Y\right)\right] \tag{5.14c}$$

where

$$\alpha(t) \equiv \dot{D} - \frac{1}{2}\left[\zeta\left(\zeta + 4\Omega_z\right) - D^2\right] \tag{5.15}$$

Note that $\alpha(t)$ is a measure of the departure from the PIO after the stall because if equation (3.8) for the PIO were enforced, $\alpha(t)$ would vanish.

Equation (5.12) is satisfied by taking

$$\nabla L = C_1(t)\mathbf{A} \tag{5.16}$$

Integrating this equation for L gives

$$L = C_1\left\{\begin{array}{l} \dfrac{\alpha}{2}\left(X^2 + Y^2\right) + \left[-D\left(\dot{x}_c - U_b\right) + \zeta\left(\dot{y}_c - V_b\right) + \dfrac{2D}{\varepsilon}\eta - 4\Omega_z V_b + 4\Omega_y \dfrac{D}{\varepsilon}\right]X \\ + \left[-\zeta\left(\dot{x}_c - U_b\right) - D\left(\dot{y}_c - V_b\right) - \dfrac{2D}{\varepsilon}\xi + 4\Omega_z U_b\right]Y + 2\left(g + \dfrac{\dot{D}}{\varepsilon} - 2\Omega_y U_b\right)Z \\ + 2\Omega_y\left(-DX + \zeta Y - \eta Z\right)Z \end{array}\right\} + C_5 \tag{5.17}$$

According to equations (5.3) and (5.8), the inner density can be written

$$\rho = (1 - B)\, \mathrm{e}^{L} \tag{5.18}$$

or

$$\rho = C_6(t)(1-B)\exp\left(C_1\left\{\begin{array}{l}\dfrac{\alpha}{2}\left(X^2+Y^2\right)+\left[-D\left(\dot{x}_c-U_b\right)+\zeta\left(\dot{y}_c-V_b\right)+\dfrac{2D}{\varepsilon}\eta-4\Omega_z V_b+4\Omega_y\dfrac{D}{\varepsilon}\right]X \\ +\left[-\zeta\left(\dot{x}_c-U_b\right)-D\left(\dot{y}_c-V_b\right)-\dfrac{2D}{\varepsilon}\xi+4\Omega_z U_b\right]Y+2\left(g+\dfrac{\dot{D}}{\varepsilon}-2\Omega_y U_b\right)Z \\ +2\Omega_y\left(-DX+\zeta Y-\eta Z\right)Z\end{array}\right\}\right) \tag{5.19}$$

The inner pressure p can now be obtained by substituting equations (5.19) and (5.14) into equation (5.6) and integrating to obtain the barotropic result

$$p = -\frac{1}{2C_1(t)}\rho \tag{5.20}$$

where ρ is given by equation (5.19). This intermediate result confirms that equations (5.13) are acceptable ODEs for the inner vorticity of a stalled-PIO model that can translate with any given velocity $\left[\dot{x}_c(t), \dot{y}_c(t)\right]$. The next step is to obtain the outer solution and apply the jump conditions at the interface to obtain equations for $\dot{a}$ and $\dot{D}$. As with the PIO model, we revert to a simplified axisymmetric, nontranslating solution that is sufficient for obtaining these two equations.

6. Axisymmetric, Nontranslating Stalled-PIO Solution

6.1. Inner Solution

The inner density (eq. (5.19)) and pressure (eq. (5.20)) for the stalled PIO become axisymmetric and nontranslating by setting $\dot{x}_c = \dot{y}_c = U_b = V_b = \xi = \eta = \Omega_y = 0$. The inner velocity fields in cylindrical coordinates are again given by equations (4.1), and the inner density becomes

$$\rho\left(r,z,t\right) = C_6(t)(1-B)\,\exp\left\{C_1(\mathrm{t})\left[\frac{1}{2}\alpha r^2+2\left(g+\frac{\dot{D}}{\varepsilon}\right)Z\right]\right\} \tag{6.1}$$

Applying the boundary condition (eq. (5.2)) at $r = a$ gives

$$C_1(t) = -\frac{\varepsilon}{2\left(g+\dfrac{\dot{D}}{\varepsilon}\right)} \tag{6.2}$$

$$C_6(t) = \sigma_b^0(t)\,\exp\left[\frac{\varepsilon\alpha a^2}{4\left(g+\dfrac{\dot{D}}{\varepsilon}\right)}\right] \tag{6.3}$$

and the inner density (eq. (6.1)) and pressure (eq. (5.20)) become

$$\rho(r,z,t) = \sigma_b^0(t)(1-B)\,\exp\left\{-\varepsilon Z + \frac{\beta}{1+\dfrac{\dot{D}}{\varepsilon g}}\left[1-\left(\frac{r}{a}\right)^2\right]\right\} \tag{6.4}$$

$$p(r,z,t) = \frac{g}{\varepsilon}\sigma_b^0(t)(1-B)\left(1+\frac{\dot{D}}{\varepsilon g}\right)\exp\left\{-\varepsilon Z + \frac{\beta}{1+\dfrac{\dot{D}}{\varepsilon g}}\left[1-\left(\frac{r}{a}\right)^2\right]\right\} \tag{6.5}$$

where β is dimensionless and defined by

$$\beta(t) = \frac{\varepsilon a^2}{4g}\alpha(t) = \frac{\varepsilon a^2}{8g}\left[2\dot{D} - \zeta\left(\zeta + 4\Omega_z\right) + D^2\right] \tag{6.6}$$

6.2. Outer Solution

The outer velocity field for the stalled-PIO model is again given by equations (4.3) and the equation for $\dot{a}$ by equation (4.4). An equation for $\dot{D}$ can be determined from the jump condition that the pressure be continuous at $r = a$. To determine the outer pressure field, we solve the momentum equation (3.3) for the pressure gradient in cylindrical coordinates and then substitute the outer velocity field from equations (4.3), ζ from equations (5.13c), and $\dot{a}$ from equation (4.4) to obtain

$$\frac{\partial p^0}{\partial r} = -\frac{g\rho^0}{\varepsilon r}\left[\gamma - F\left(\frac{a}{r}\right)^2\right] \tag{6.7a}$$

$$\frac{\partial p^0}{\partial \theta} = 0 \tag{6.7b}$$

$$\frac{\partial p^0}{\partial z} = -g\rho^0 \tag{6.7c}$$

where F is given by (4.6) and

$$\gamma(t) = \frac{\varepsilon a^2}{2g}\left(\dot{D} - 2\Omega_z\zeta + D^2\right) \tag{6.8}$$

For the PIO, F was a constant of the motion; however, after the stall, F becomes time-dependent.

Again we impose equation (4.7), so the outer density ρ^0 must satisfy

$$\frac{\partial \rho^0}{\partial r} - \frac{1}{\varepsilon r}\left[\gamma - F\left(\frac{a}{r}\right)^2\right]\frac{\partial \rho^0}{\partial z} = 0 \tag{6.9}$$

The solution of this equation that satisfies the boundary condition (eq. (5.1)) at $r = a$ is given by

$$\rho^0(r,z,t) = \sigma_b^0 \left(\frac{a}{r}\right)^\gamma \exp\left\{-\varepsilon Z + \frac{F}{2}\left[1 - \left(\frac{a}{r}\right)^2\right]\right\} \tag{6.10}$$

where we must have $\gamma \geq 0$ for $\rho^0(r,z,t)$ to remain bounded as $r \to \infty$. Substituting this result in equation (6.7) and integrating for the outer pressure, we obtain the hydrostatic result

$$p^0(r,z,t) = \frac{g}{\varepsilon}\rho^0(r,z,t) = \sigma_b^0 \frac{g}{\varepsilon}\left(\frac{a}{r}\right)^\gamma \exp\left\{-\varepsilon Z + \frac{F}{2}\left[1 - \left(\frac{a}{r}\right)^2\right]\right\} \tag{6.11}$$

For the PIO, $p^0(r,z,t)$ and $\rho^0(r,z,t)$ had maximum values at $r = a$; however, for the stalled PIO, these maxima occur at radius $r_{\max}$, where

$$r_{\max} = a\left(\frac{F}{\gamma}\right)^{1/2} \tag{6.12}$$

Again we identify these maximum values $p^0(r_{\max}, b)$ and $\rho^0(r_{\max}, b)$ at height b with the environmental pressure p_b^{envir} and environmental density ρ_b^{envir} at height b, which are constants. If we substitute the radius given by equation (6.12) into the outer pressure (eq. (6.11)) at height $z = b$, we can solve for $\sigma_b^0(t)$

$$\sigma_b^0(t) = \rho_b^{\text{envir}}\left(\frac{F}{\gamma}\right)^{\frac{\gamma}{2}} \exp\left[\frac{1}{2}(\gamma - F)\right] = p_b^{\text{envir}}\frac{\varepsilon}{g}\left(\frac{F}{\gamma}\right)^{\frac{\gamma}{2}} \exp\left[\frac{1}{2}(\gamma - F)\right] \tag{6.13}$$

and the outer pressure (eq. (6.11)) and inner pressure (eq. (6.5)) become

$$p^0(r,z,t) = \frac{g}{\varepsilon}\rho^0(r,z,t) = p_b^{\text{envir}}\left(\frac{F}{\gamma}\right)^{\frac{\gamma}{2}}\left(\frac{a}{r}\right)^\gamma \exp\left\{-\varepsilon Z + \frac{1}{2}\left[\gamma - F\left(\frac{a}{r}\right)^2\right]\right\} \tag{6.14}$$

and

$$p = p_b^{\text{envir}}(1-B)\left(1 + \frac{\dot{D}}{\varepsilon g}\right)\left(\frac{F}{\gamma}\right)^{\frac{\gamma}{2}} \exp\left\{-\varepsilon Z + \frac{1}{2}(\gamma - F) + \frac{\beta}{1 + \frac{\dot{D}}{\varepsilon g}}\left[1 - \left(\frac{r}{a}\right)^2\right]\right\} \tag{6.15}$$

6.3. *Buoyancy and* $\dot{D}$

By equating the outer pressure (eq. (6.14)) and the inner pressure (eq. (6.15)) at $r = a$, we again obtain the result (eq. (4.15)); but now, after the stall, the buoyancy $B(t)$ is given, and w (or D) is determined

by integrating this equation. After the stall, equations (4.22) and (4.23) for the outer and inner temperatures also remain valid. With equation (4.15) substituted, the inner pressure (eq. (6.15)) becomes

$$p(r,z,t) = p_b^{\text{envir}} \left(\frac{F}{\gamma}\right)^{\frac{\gamma}{2}} \exp\left\{-\varepsilon Z + \frac{1}{2}(\gamma - F) + \lambda\left[1 - \left(\frac{r}{a}\right)^2\right]\right\} \tag{6.16}$$

where

$$\lambda(t) = \beta(1-B) = \frac{\varepsilon a^2}{8g}\left\{2\varepsilon g B - (1-B)\left[\zeta\left(\zeta + 4\Omega_z\right) - D^2\right]\right\} \tag{6.17}$$

and now

$$\gamma(t) = \frac{\varepsilon a^2}{2g}\left(\varepsilon g B - 2\Omega_z \zeta + D^2\right) \tag{6.18}$$

We substitute equations (6.16) and (4.23) into equation (4.25) and integrate over the volume of the core to obtain the thermal input power

$$\begin{aligned} Q^{\text{stalled PIO}} = {} & p_b^{\text{envir}} \frac{\pi a^2}{\varepsilon}\left(\frac{F}{\gamma}\right)^{\frac{\gamma}{2}} \left\{\exp\left[\frac{1}{2}(\gamma - F)\right]\right\} \left\{1 - \exp\left[-\varepsilon(h-b)\right]\right\} \\ & \times \left\{\left[\frac{\varepsilon}{g} c_p T^0 \dot{B} + D\left(\frac{c_p}{g}\frac{\mathrm{d}T^0}{\mathrm{d}z} + 1\right) - \frac{\dot{F}}{2}\left(\frac{\gamma}{F} - 1\right) - \frac{\dot{\gamma}}{2}\ln\left(\frac{F}{\gamma}\right)\right]\frac{\left(\mathrm{e}^{\lambda} - 1\right)}{\lambda} + \frac{\dot{\lambda}}{\lambda^2}\left[\mathrm{e}^{\lambda}(1-\lambda) - 1\right]\right\} \end{aligned} \tag{6.19}$$

By equations (6.4), (4.15), and (6.17), the inner density ρ is given by

$$\rho(r,z,t) = \frac{\varepsilon}{g}(1-B)p(r,z,t) = p_b^{\text{envir}}(1-B)\frac{\varepsilon}{g}\left(\frac{F}{\gamma}\right)^{\frac{\gamma}{2}} \exp\left\{-\varepsilon Z + \frac{1}{2}(\gamma - F) + \lambda\left[1 - \left(\frac{r}{a}\right)^2\right]\right\} \tag{6.20}$$

and by comparison with equation (5.3)

$$\sigma(r,t) = p_b^{\text{envir}} \frac{\varepsilon}{g}\left(\frac{F}{\gamma}\right)^{\frac{\gamma}{2}} \exp\left\{\frac{1}{2}(\gamma - F) + \lambda\left[1 - \left(\frac{r}{a}\right)^2\right]\right\} \tag{6.21}$$

Substituting equation (6.21) into equation (5.5) gives for the ratio

$$R_{\text{DHD approx}}^{\text{stalled PIO}}(r,t) = \left|\frac{1}{D}\left\{\dot{B} - \frac{\dot{F}}{2}\left(\frac{\gamma}{F} - 1\right) - \frac{\dot{\gamma}}{2}\ln\left(\frac{F}{\gamma}\right) - \dot{\lambda}\left[1 - \left(\frac{r}{a}\right)^2\right]\right\}\right| \tag{6.22}$$

Because this ratio depends upon r, we will evaluate it during model runs at $r = 0$, $r = 0.707a$, and $r = a$ and choose the maximum (i.e., conservative) value. The cloud-base mass influx after the stall is obtained by substituting equation (6.20) into equation (4.19).

$$M^{\text{stalled PIO}} = \frac{\pi}{g} a^2 D(1-B) p_b^{\text{envir}} \left(\frac{F}{\gamma}\right)^{\frac{\gamma}{2}} \exp\left[\frac{1}{2}(\gamma - F)\right] \frac{1}{\lambda}\left(e^{\lambda} - 1\right) \tag{6.23}$$

6.4. Central Pressure Deficit

The environmental pressure $p^{\text{envir}}(z)$ is obtained as a function of height by substituting equation (6.12) into equation (6.14)

$$p^{\text{envir}}(z) = p_b^{\text{envir}} \mathrm{e}^{-\varepsilon Z} \tag{6.24}$$

We find the minimum internal pressure $p_{\min}(z,t)$ at the center of the mesocyclone, which is now becoming a tornadic cyclone, by setting $r = 0$ in equation (6.16)

$$p_{\min}(z,t) = p_b^{\text{envir}} \left(\frac{F}{\gamma}\right)^{\frac{\gamma}{2}} \exp\left[-\varepsilon Z + \lambda + \frac{1}{2}(\gamma - F)\right] \tag{6.25}$$

The central pressure deficit $\Delta p(z,t)$ is defined as

$$\Delta p(z,t) = p^{\text{envir}}(z) - p_{\min}(z,t) \tag{6.26}$$

or

$$\Delta p(z,t) = p_b^{\text{envir}} \mathrm{e}^{-\varepsilon Z} \left\{1 - \left(\frac{F}{\gamma}\right)^{\frac{\gamma}{2}} \exp\left[\lambda + \frac{1}{2}(\gamma - F)\right]\right\} \tag{6.27}$$

where λ, γ, and F are given by equations (6.17), (6.18), and (4.6), respectively. In our calculations, we will always evaluate Δp at height b where $Z = 0$.

7. Tornadic Cyclone Solution

7.1. Constant B After Stall

Figure 4 shows the stalled-PIO solution for Tornadic Cyclone A9, where the truncated value of B is held constant after the stall that starts at $t \approx 21$ min. The environmental parameters are given in table 1 and the initial values in table 3. (Purely for pedagogy, this figure also shows the plots for a fictitious unstalled PIO where ΔT unrealistically reaches +96 K.) The truncated buoyancy shown in figure 4(a) is insufficient to cause the rapid draft reversal required by the PIO (fig. 4(b)), so the contracting downdraft is prolonged, as shown in figures 4(b) and (c). Prolongation of the contracting downdraft spins up the Rossby number well above the tornadic cyclone value of $\mathrm{Ro} \approx 1000$, as shown in figure 4(d). The ratio

$R_{\text{DHD approx}}$ from equations (2.7) and (6.22) is plotted in figure 4(e). This ratio is small, except for a brief interval when it reaches 0.28 just before the stall begins. Therefore, the DHD approximation was reasonably accurate during this segment of the calculation.

The prolonged downdraft of the stalled-PIO model is in qualitative agreement with the collapsing phase of a supercell storm, as described by Rotunno (1986): "The BWER [bounded weak echo region] begins to fill, and downdrafts intensify ... . In association with this development, a tornado forms at full strength and may last from a few to several tens of minutes." The prolonged downdraft is also in agreement with more recent observations by Trapp (2000) of weak-to-moderate downflow throughout the entire depth of a mesocyclone just before tornadogenesis. It is also in agreement with early observations by Fujita (1972) that tornadoes are most likely to occur during a decrease in the height of clouds that overshoot the top of a supercell.

The mesocyclonic circulation Γ is plotted in figure 4(f), where it again achieves the value $\Gamma_{\max} = 5 \times 10^5 \text{ m}^2 \text{ s}^{-1}$. The initial values for ζ and D in table 3 were chosen so that $\Gamma \approx 0$ at $t = 0$. The cloud base mass influx M is plotted in figure 4(g) and the thermal input power Q in figure 4(h). Both of these quantities go through zero at maximum spin-up when w goes through zero.

The central pressure deficit is computed from equation (6.27) at height $z = b$ and is plotted in figure 4(i). Before the stall, we see that $\Delta p = 0$, which is consistent with inertial flow. After the stall, Δp builds to a value that substantially exceeds the maximum measured value of 34 mb. The radial dependence of the pressure at height $z = b$ is plotted in figure 4(j) before the stall and at various times after the stall. These plots were computed from equation (6.16) for $r \le a$ and from equation (6.14) for $r \ge a$.

7.2. Extending Lifetime of Simulated Tornadic Cyclone

An obvious shortcoming of our simulated tornadic cyclone is that it lasts for only about 4 min, while Tornadic Cyclone A9 lasted for 80 min. According to figures 4(b)–(d), the simulated tornadic cyclone began to expand and spin down when w became positive at $t \approx 25.7$ min. However, should we prescribe that the buoyancy $B \to 0$ as $w \to 0$, then by equations (2.5), (4.15), and (5.13c), it follows that $D, \dot{w}, \dot{D}$, and $\zeta \to 0$ also, and the simulation would stay in a state of maximum spin-up indefinitely. (Recall that for an actual storm, $B = w = 0$ means that the average buoyancy and average vertical flow would remain zero; that is, the updrafts and downdrafts would remain in balance.)

We can try to apply this intuitive argument to our mathematical solution. However, should we set $B = w = D = \dot{D} = \dot{\zeta} = 0$, we immediately encounter two problems: (a) as given by equation (6.18), γ would then be negative and our solution would lose its validity because the outer pressure (eq. (6.14)) would become unbounded as $r \to \infty$; and (b) the DHD approximation would become inaccurate because the ratio $R_{\text{DHD approx}}$, as given by equation (6.22), could become very large. To solve problem (a), we will assume that when $\text{Ro} \ge 1000$, we may neglect the Coriolis force by letting $\Omega_z \to 0$ so that the troublesome term $-2\Omega_z\zeta$ disappears from equation (6.18). The transition from inertial to cyclostrophic flow that occurs after the stall supports this assumption. We can ameliorate problem (b) by specifying that as $B \to 0$, $D \to -1.875 \times 10^{-5} \text{ s}^{-1}$ instead of going to zero, which corresponds to $w \to -0.158 \text{ m s}^{-1}$. Although the core continues to contract, Ro increases by less than 10 percent during the 80-min simulated lifetime, and the DHD approximation remains reasonably accurate.

Implementing this approach after the stall, we replace the constant B with

$$B'(t) = \frac{12}{288.6}\left[1 - H_n\left(t - t_0\right)\right] \tag{7.1}$$

and the constant Ω_z with

$$\Omega_z'(t) = \Omega_z\left[1 - H_n\left(t - t_0\right)\right] \tag{7.2}$$

where $H_n(t)$ is a smoothed Heaviside unit step function defined by

$$H_n(t) = \frac{1}{2}\left[1 + \tanh(nt)\right] \tag{7.3}$$

The values $n = 0.011111$ and $t_0 = 1543.7$ s provide a smooth transition and achieve the target value for D (or w) given previously. The resultant plots for a sustained tornadic cyclone are shown in figure 5. During the sustained period ($t > 30$ min), the values for M and Q are relatively small ($M \approx -6 \times 10^5$ kg s^{-1} and $Q \approx -3 \times 10^9$ W) because the updrafts and downdrafts are nearly in balance.

7.3. Terminating the Tornadic Cyclone

We shall now attempt to simulate the observed termination of Tornadic Cyclone A9 after 80 min. Our strategy is to use $B(t)$ to induce a positive pulse in $D(t)$ or $w(t)$ that will cause the core to expand and spin down, after which w also returns to zero. This approach requires $B(t)$ to make a positive excursion followed by an equal negative excursion. But again we encounter problems: (a) because γ goes negative during the negative excursion of $B(t)$ and (b) because $R_{\text{DHD approx}}$ has an infinite pole where $D(t)$ goes through zero at the onset of its positive pulse.

We can prevent the problem with γ by decreasing the negative excursion of $B(t)$, which has the consequence of leaving D (or w) in a somewhat elevated or nonzero final state—which turns out to be fortuitous. Because $R_{\text{DHD approx}}$, as given by equation (6.22), is a function of both r and t, we cannot circumvent its pole at $t \approx 103$ min by further tailoring $B(t)$. However, we can argue that the ratio $R_{\text{DHD approx}}$ as defined by equation (6.22) could be too severe a test of the DHD approximation, because anytime that D passes through zero, we risk such a pole. Regardless, we will proceed so that the model will conform to the data.

After the stall, the complete buoyancy is given by

$$B''(t) = \frac{12}{288.6}\left\{1 - H_n\left(t - t_0\right) + \frac{1.8}{\sqrt{3}}\left[H_m\left(t - t_1\right) - 3H_m^2\left(t - t_1\right) + 2H_m^3\left(t - t_1\right)\right]\left[1 - kH_s\left(t - t_1\right)\right]\right\} \tag{7.4}$$

where $n = 0.011111$, $m = 0.005$, $s = 1$, $t_0 = 1543.7$ s, $t_1 = 6761$ s, and $k = 0.7432$. On the right-hand side, the first two terms are the same as in equation (7.1), the third degree polynomial in $H_m\left(t - t_1\right)$ gives the terminating bipolar excursion, and the right-most factor decreases the negative part of this excursion.

For further discussion of polynomials and generalized functions based on the hyperbolic tangent form of $H_n(t)$, see Costen (1967).

The complete simulation of Tornadic Cyclone A9 is plotted in figure 6. It is apparent from figure 6(a) that we have sought a small perturbation in buoyancy that would be effective in terminating the tornadic cyclone. An enlargement of this perturbation is shown in figure 7(a). The effects on w and a are shown in figures 6(b) and 6(c). The final elevated value of w causes an increase in a and dramatic declines in both Ro and Δp, as shown in figures 6(d) and 6(e). The ratio $R_{\text{DHD approx}}$ is plotted in figure 6(f). The pole at $t \approx 103$ min coincides with the final ascent of w through zero. The discontinuity in $R_{\text{DHD approx}}$ at $t \approx 113$ min results from the discontinuity in $\dot{B}$ that occurs between the positive and negative lobes of ΔT, as shown in figure 7(a).

The mesocyclonic circulation Γ, as shown in figure 6(g), is unaffected during termination, which confirms that the declines in Ro and Δp are the result of core expansion from the induced updraft. The mass influx at cloud base M is plotted in figure 6(h). The increase in M that results from the expanding updraft is seen by enlarging the last 40 min, as shown in figure 7(b). Near the end, the computed value for M is rapidly increasing and, if the computation continued further, M would soon reach the measured reference value $M_{\text{ref}} = 1.2 \times 10^9$ kg s^{-1} reported by Foote and Fankhauser (1973) for a different supercell. The thermal input power Q is shown in figure 6(i), and a similar enlargement is shown in figure 7(c), where the discontinuity in Q again marks the end of the positive lobe of ΔT. Like M, Q is rapidly increasing, and if the computation continued further, Q would soon reach the measured reference value $Q_{\text{ref}} = 1.9 \times 10^{13}$ W.

During the prolonged phase of the model tornadic cyclone, $\Delta T = 0$ and $w = -0.158$ m s^{-1}. Since these quantities represent average values for an actual storm, we infer that storm longevity requires the updrafts and downdrafts to be essentially equal in magnitude and the positive buoyancy that drives the updrafts to be in balance with the negative buoyancy that drives the downdrafts. According to the model, termination of the tornadic cyclone requires a thermal input that warms and intensifies the updrafts, warms and diminishes the downdrafts, or both. In nature, this thermal input would result from increased condensational heating, decreased evaporative cooling, or both. This model-based concept of weakening a tornadic cyclone by the application of heat is consistent with the observed weakening of tornadic storms that move from land to water, which is a source of additional heat.

Following Kessler (1972) and others, we speculate how human beings might intervene to trigger the termination process earlier. According to figures 7(a) and 7(c), the positive lobe of ΔT results from a thermal power input of 11-min duration that peaks at 158 GW. The average power input is 61 GW, and the total thermal energy deposited into the tornadic cyclone is 40 TJ. As a result of this thermal input, w increases from −0.158 m s^{-1} to +10 m s^{-1}. The negative lobe of ΔT subsequently reduces w to +8 m s^{-1}, and this sustained average updraft causes the core to expand and spin down quickly.

Suppose that we were able to manually input 40 TJ of thermal energy into the tornadic cyclone at some earlier time with the result that w is increased to 10 m s^{-1}. In a convectively unstable troposphere, this new value for w could be sustained naturally by latent energy release without further manual input. If the new value for w were sustained, we would have successfully triggered the termination process. Selectively injecting this thermal energy into the downdrafts would avoid augmenting the production of hail.

Our value 40 TJ (or 11 million kWh) is an order of magnitude lower than Kessler's (1972) estimated input energy of 80 million kWh to prevent the initial development of a supercell storm. At a rate of 0.1 USD per kWh, 40 TJ would cost 1 million USD. This expenditure compares favorably with the 1 billion USD property damage plus injuries and loss of life incurred by Tornado A9.

The model also provides insight into forecasting which supercell storms will develop a tornadic cyclone and produce strong tornadoes. If the supercell conforms to the PIO model, it can produce hail but not strong tornadoes. Therefore, if Doppler radar images show that parcels in the core are following inertial trajectories (as projected on a horizontal plane), the supercell will not produce a strong tornado. However, should the core trajectories transition from inertial to cyclostrophic, the forecaster can infer that the PIO has stalled and that the formation of a tornadic cyclone and a strong tornado is likely.

8. Concluding Remarks

Unlike the PIO model or the conventional splitting-storm model, the stalled-PIO model is capable of simulating a tornadic cyclone that originates in the midtropospheric layer—in agreement with radar observations of the strongest tornadic storms. After the PIO model became stalled in a state of contraction and spin-up, we were able to tailor the buoyancy in the core so that the stalled-PIO model simulated the 80-min lifetime of intense Tornadic Cyclone A9 that occurred over Oklahoma City, Oklahoma, on May 3, 1999.

The dilatation-horizontal divergence (DHD) approximation used in the PIO and stalled-PIO models states that the horizontal divergence in the cylindrical core is predominantly due to the three-dimensional dilatation of rising/falling air parcels. Thus, the horizontal divergence is approximately equal to the updraft speed divided by the scale height. To check the accuracy of this approximation during our model runs, we plotted the ratio of neglected terms to retained terms in the continuity equation. This check was quite severe because whenever the horizontal divergence passed through zero, the plotted ratio could blow up. Such a blowup occurred once, but it was near the end of the run when the tornadic cyclone was decaying. Twice the ratio approached the value 0.3, although most of the time the ratio was much less than 0.1. We conclude that the DHD approximation was reasonably accurate during our PIO and stalled-PIO model runs.

The model tornadic cyclone remained in a nearly steady state when the spatial average buoyancy, average vertical flow, and average thermal input from latent energy release were close to zero, that is, when the updrafts and downdrafts were in balance. The tornadic cyclone was terminated by a predominantly positive pulse of buoyancy that increased the average vertical speed to 8 m s^{-1}. As a consequence of the DHD approximation, this sustained updraft caused the tornadic cyclone to expand and spin down rapidly.

The terminating buoyant pulse required a thermal input of 40 TJ or 11 million kWh. For Tornadic Cyclone A9, this thermal input was supplied by latent energy release. However, we could, in principle, manually inject this thermal energy to trigger an early termination of the tornadic cyclone and its pendant tornado. Our calculated energy value of 40 TJ is an order of magnitude less than previous model-based estimates for effective human intervention.

9. References

Bengtsson, L.; and Lighthill, J. (Ed.) 1982: *Intense Atmospheric Vortices.* Springer-Verlag.

Brandes, E. A. 1981: Fine Structure of the Del City-Edmond Tornadic Mesocirculation. *Mon. Wea. Rev.*, vol. 109, pp. 635–647.

Burgess, D. W.; and Magsig, M. A. 2000: Understanding WSR-88D Signatures for the 3 May 1999 Oklahoma City Tornado. *20th AMS Conference on Severe Local Storms,* 11–15 Sep. 2000, Orlando, FL, Amer. Meteor. Soc.

Church, C.; Burgess, D.; Doswell, C.; and Davies-Jones, R. (Ed.) 1993: *The Tornado: Its Structure, Dynamics, Prediction, and Hazards.* Geophysical Monograph 79, American Geophysical Union.

Costen, R. C. 1967: *Products of Some Generalized Functions*. NASA TN D-4244.

Costen, R. C.; and Miller, L. J. 1998: Pulsing Inertial Oscillation, Supercell Storms, and Surface Mesonetwork Data. *J. Engr. Math.* vol. 34, pp. 277–299.

Costen, R. C.; and Stock, L. V. 1992: *Inertial Oscillation of a Vertical Rotating Draft With Application to a Supercell Storm*. NASA TP-3230 with 8-minute video supplement available.

Darkow, G. L. 1986: Basic Thunderstorm Energetics and Thermodynamics. *Thunderstorm Morphology and Dynamics.* Second ed., E. Kessler, ed., Vol. 2. *Thunderstorms: A Social, Scientific, and Technological Documentary*. Univ. of Oklahoma Press, London, pp. 59–73.

Davies-Jones, R. P. 1986: Tornado Dynamics. *Thunderstorm Morphology and Dynamics*, Second ed., E. Kessler, ed., Vol. 2. *Thunderstorms: A Social, Scientific, and Technological Documentary.* Univ. of Oklahoma Press, pp. 197–236.

Doswell, C. A. III (Ed.) 2001: Severe Convective Storms. *Meteror. Monogr.*, vol. 28, no. 50, Amer. Meteor. Soc.

Edwards, R.; and Thompson, R. L. 2000: Initiation of Storm A (3 May 1999) Along a Possible Horizontal Convective Roll. *20th AMS Conference on Severe Local Storms,* 11–15 Sep. 2000, Orlando, FL, Amer. Meteor. Soc.

Ferrel, W. 1889: *A Popular Treatise on the Winds*. John Wiley, 505 pp.

Foote, G. B.; and Fankhauser, J. C. 1973: Airflow and Moisture Budget Beneath a Northeast Colorado Hailstorm. *J. Appl. Meteor.*, vol. 12, pp. 1330–1353.

Fujita, T. T. 1972: Tornado Occurrences Related to Overshooting Cloud-Top Heights as Determined From ATS Pictures. *Satellite & Mesometeorology Research Project, Research Paper 97*. The Univ. of Chicago, 32 pp.

Fujita, T. T. 1973: Tornadoes Around the World. *Weatherwise*, vol. 26, pp. 56–83.

Haltiner, G. J.; and Martin, F. L. 1957: *Dynamical and Physical Meteorology.* McGraw-Hill, 470 pp.

Holton, J. R. 1992: *An Introduction to Dynamic Meteorology*. Third ed., Academic Press.

Kessler, E. 1972: On Tornadoes and Their Modification. *Technology Rev.*, May, pp. 48–55.

Kessler, E. (Ed.) 1986: *Thunderstorm Morphology and Dynamics.* Second ed. Vol. 2. *Thunderstorms: A Social, Scientific, and Technological Documentary.* Univ. of Oklahoma Press.

Klemp, J. B. 1987: Dynamics of Tornadic Thunderstorms. *Ann. Rev. Fluid Mech*., vol. 19, pp. 369–402.

Lilly, D. K. 1986: The Structure, Energetics and Propagation of Rotating Convective Storms. Part II: Helicity and Storm Stabilization. *J. Atmos. Sci*., vol. 43, pp. 126–140.

Maddox, R. A. 1976: An Evaluation of Tornado Proximity Wind and Stability Data. *Mon. Wea. Rev*., vol. 104, pp. 133–142.

Menke, W.; and Abbott, D. 1990: *Geophysical Theory*. Columbia Univ. Press, New York, 458 pp.

Miller, L. J.; Tuttle, J. D., and Knight, C. A. 1988: Airflow and Hail Growth in a Severe Northern High Plains Supercell. *J. Atmos. Sci*., vol. 45, pp. 736–762.

Morton, B. R. 1966: Geophysical Vortices. *Progress in Aero. Sci*., vol. 7 (ed. D. Kuchemann), Pergamon Press, pp. 145–194.

Ray, P. S. (Ed.) 1986: *Mesoscale Meteorology and Forecasting.* Amer. Meteor. Soc.

Rotunno, R. 1986: Tornadoes and Tornadogenesis, Chapter 18, P. S. Ray (Ed.). *Mesoscale Meteorology and Forecasting.* Amer. Meteor. Soc.

Rotunno, R.; and Klemp, J. B. 1982: The Influence of the Shear-Induced Pressure Gradient on Thunderstorm Motion. *Mon. Wea. Rev*., vol. 110, pp. 136–151.

Schlesinger, R. E. 1980: A Three-Dimensional Numerical Model of an Isolated Deep Thunderstorm. Part II: Dynamics of Updraft Splitting and Mesovortex Couplet Evolution. J. Atmos. Sci., vol. 37, pp. 395–420.

Trapp, R. J. 2000: A Clarification of Vortex Breakdown and Tornadogenesis. *Mon. Wea. Rev*., vol. 128, pp. 888–894.

Trapp, R. J.; and Davies-Jones, R. 1997: Tornadogenesis With and Without a Dynamic Pipe Effect. *J. Atmos. Sci*., vol. 54, pp. 113–133.

Vasiloff, S. V. 1993: Single-Doppler Radar Study of a Variety of Tornado Types. Church, C.; Burgess, D.; Doswell, C.; and Davies-Jones, R. (Ed.) 1993: *The Tornado: Its Structure, Dynamics, Prediction, and Hazards*. Geophysical Monograph 79, American Geophysical Union, pp. 223–231.

Wallace, J. M.; and Hobbs, P. V. 1977: *Atmospheric Science, An Introductory Survey.* Academic Press.

Wicker, L. J.; and Wilhelmson, R. B. 1995: Simulation and Analysis of Tornado Development and Decay Within a Three-Dimensional Supercell Thunderstorm. *J. Atmos. Sci*., vol. 52, pp. 2675–2703.

Wilhelmson, R. B.; and Wicker, L. J. 2001: Numerical Modeling of Severe Local Storms. Doswell, C. A. III (Ed.) 2001: Severe Convective Storms. *Meteor. Monogr*., vol. 28, no. 50, Amer. Meteor. Soc., pp. 123–166.

Table 1. Parameters Used in PIO and Stalled-PIO Models for Tornadic Cyclone A9, Where Meteorological Values Are From Edwards and Thompson (2000) and Burgess and Magsig (2000).

Ω_z, rad s^{-1}	4.114×10^{-5}
b, km MSL	1.727
h, km MSL	7.810
p_b^{envir}, kPa	82
ε, m^{-1}	1.1842×10^{-4}
$T^0(b)$, K	288.6
dT^0/dz, K m^{-1}	-8×10^{-3}
g, m s^{-2}	9.81
R, J kg^{-1} K^{-1}	287
c_p, J kg^{-1} K^{-1}	1004
L_c, J kg^{-1}	2.5×10^6

Table 2. Initial Values Used in Maximal PIO Model Run (Figs. 1 and 3), Where $(-12 \text{ K} \le \Delta T \le 12 \text{ K})$ and $\Gamma_{max} = 5 \times 10^5$ m^2 s^{-1}

$\zeta(0)$, s^{-1}	-5.0748×10^{-5}
$D(0)$, s^{-1}	-5.4972×10^{-4}
$a(0)$, km	71.344656

Table 3. Initial Values Used in Fictitious PIO Model (Fig. 4), Where $(-12 \text{ K} \le \Delta T \le 96 \text{ K})$, and Stalled-PIO Model (Figs. 4 to 7), Where $(-12 \text{ K} \le \Delta T \le 12 \text{ K})$ and $\Gamma_{max} = 5 \times 10^5$ m^2 s^{-1}

$\zeta(0)$, s^{-1}	-1.03956×10^{-8}
$D(0)$, s^{-1}	-1.50804×10^{-3}
$a(0)$, km	43.9939

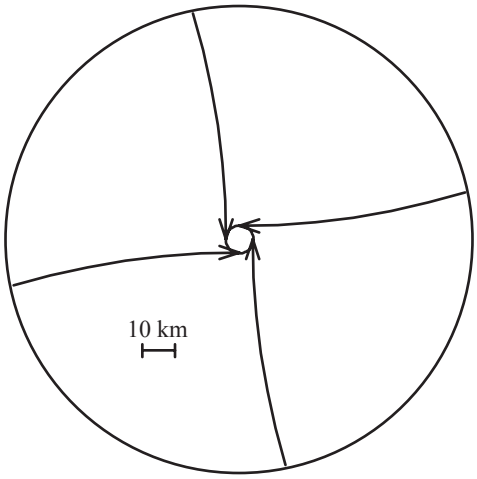

(a) Contraction and spin-up during first hour.

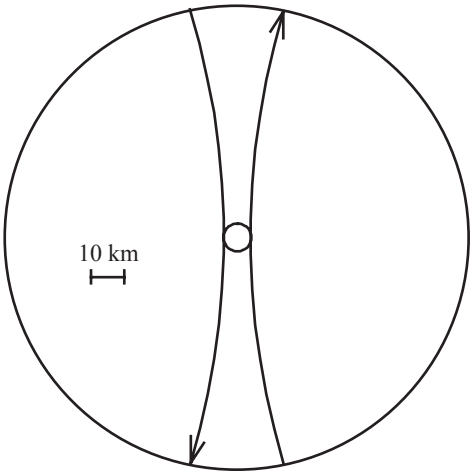

(b) Two-hr trajectories.

Figure 1. Aerial view showing inertial trajectories of parcels on core periphery during 2-hr period centered on maximal PIO pulse. (See also fig. 3.)

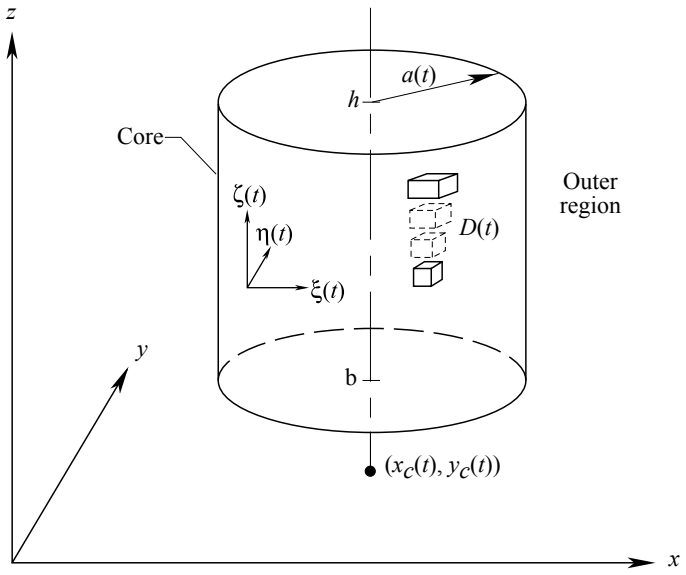

Figure 2. Pulsing inertial oscillation (PIO) model or stalled-PIO model for convective core of supercell storm or tornadic cyclone. The core radius is $a(t)$ and centerline is located at $\left[x_c(t), y_c(t)\right]$. The horizontal divergence $D(t)$, buoyancy $B(t)$, and vertical components of vorticity $\zeta(t)$ and velocity $w(t)$ are uniform inside core and zero in outer region. The midtropospheric layer extends from heights b to h.

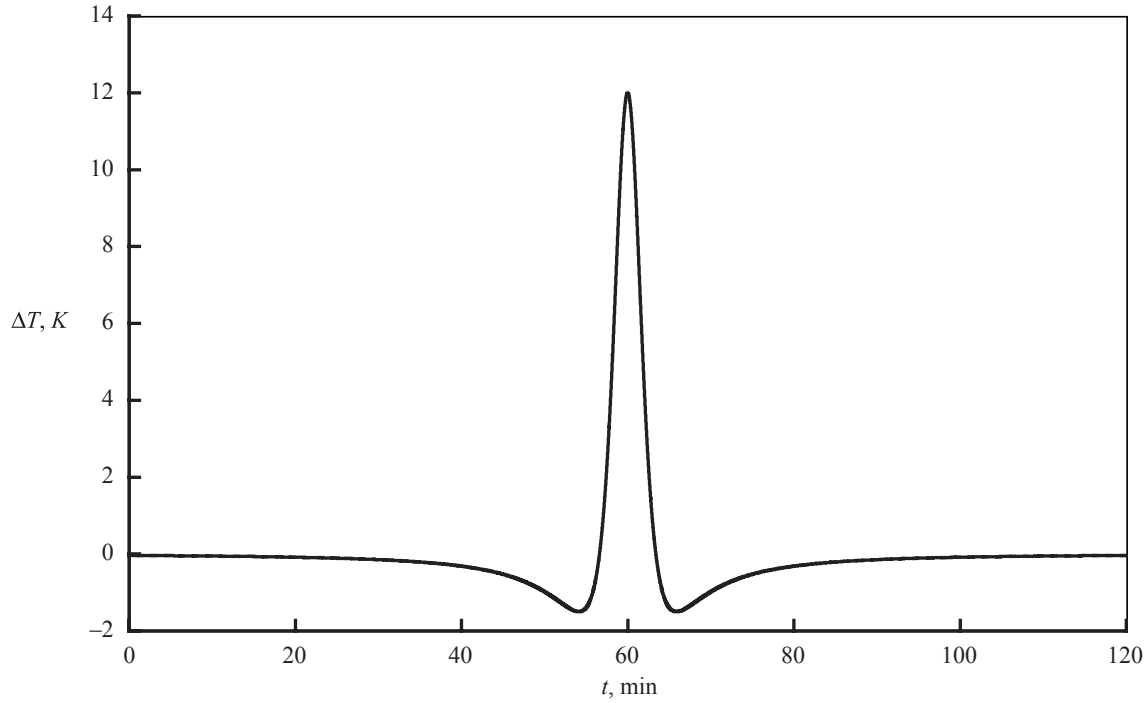

(a) Core temperature excess ΔT versus t.

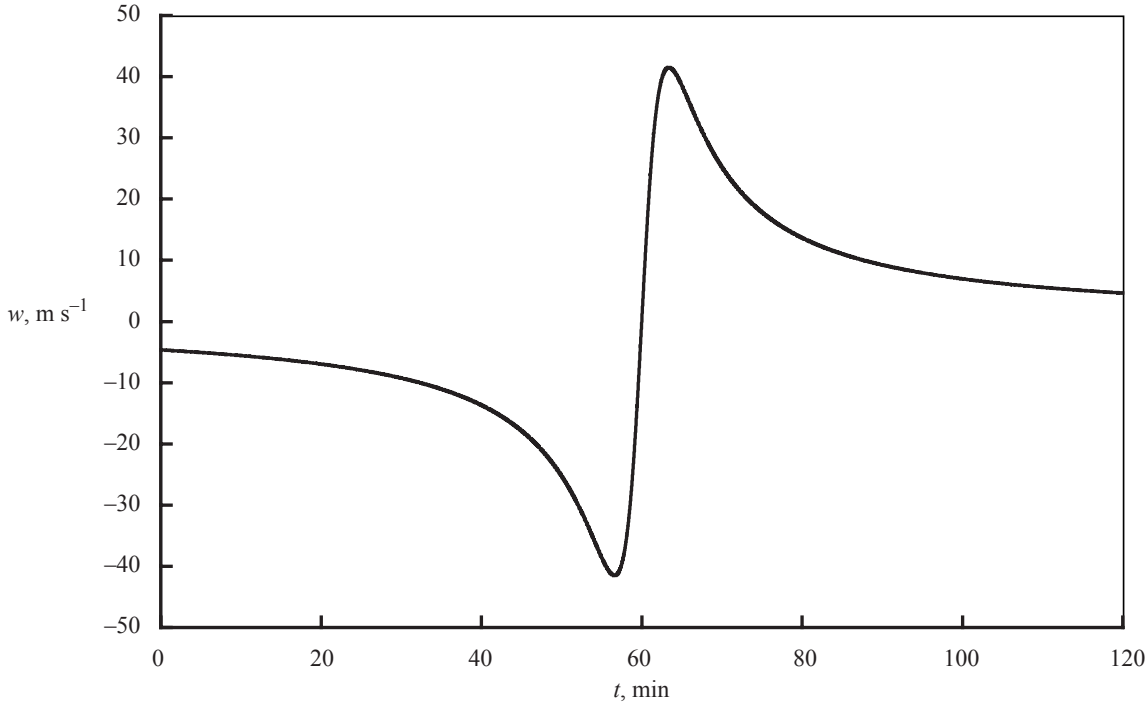

(b) Updraft speed w versus t.

Figure 3. Maximal PIO plots during 2-hr period centered on pulse. (See also fig. 1.) As in all runs, mesocyclonic circulation at maximum contraction and spin-up has value $\Gamma_{max} = 5 \times 10^5 \text{ m}^2 \text{ s}^{-1}$.

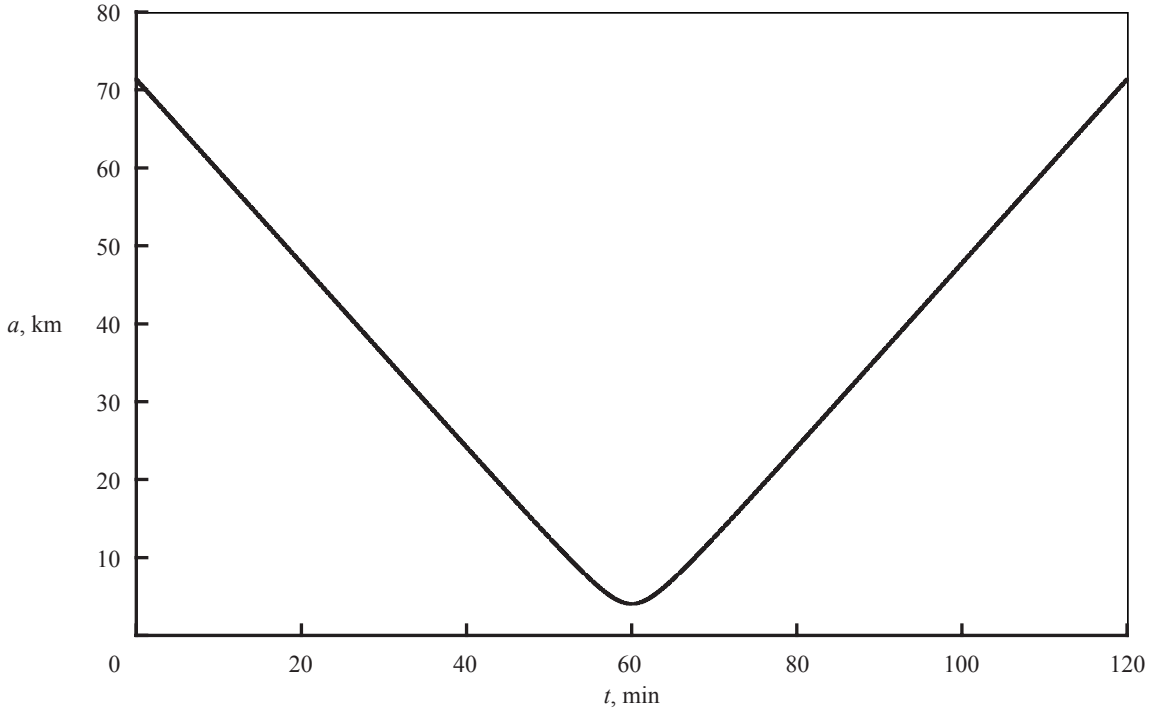

(c) Core radius a versus t.

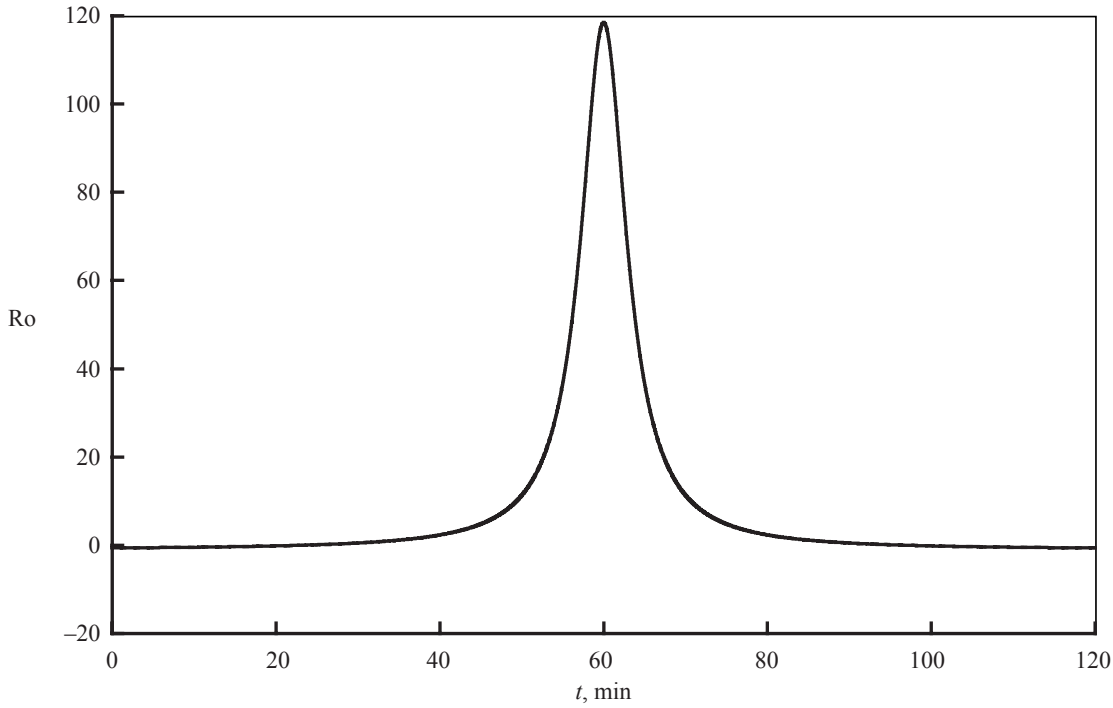

(d) Rossby number Ro versus t. (See eq. (3.2).)

Figure 3. Continued.

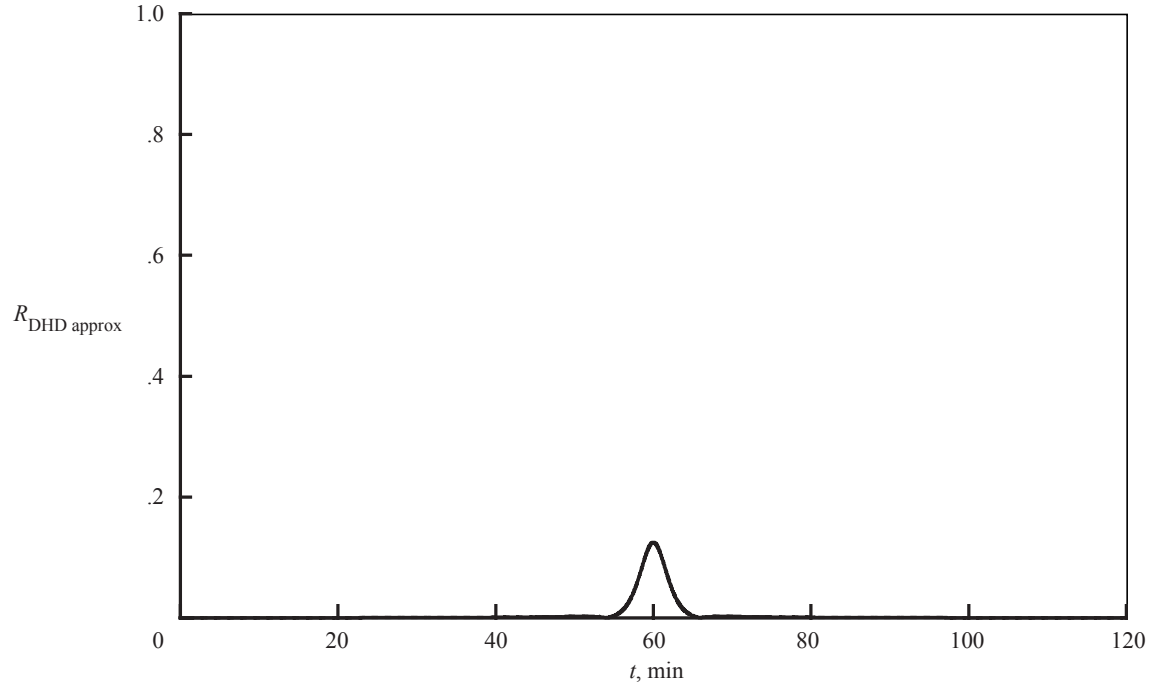

(e) Ratio $R_{\text{DHD approx}}$ of neglected terms to retained terms in dilatation-horizontal divergence (DHD) approximation (eq. (2.5)) versus t. (See eq. (2.7).)

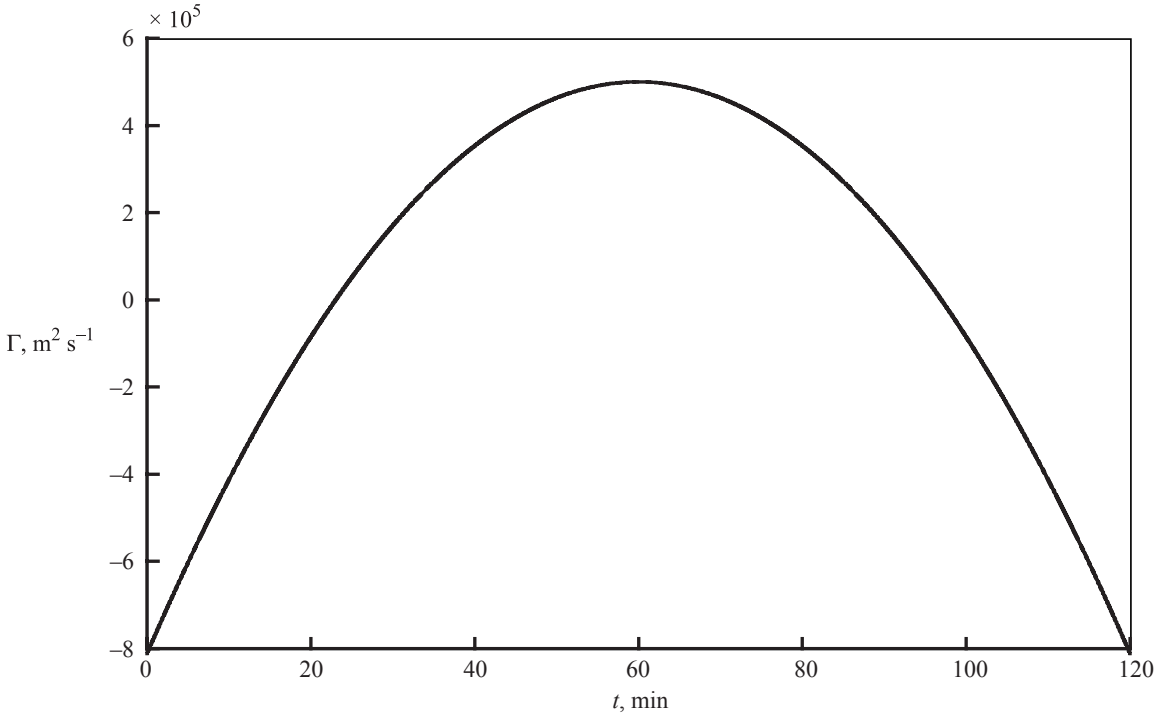

(f) Mesocyclonic circulation Γ versus t. (See eq. (4.18).)

Figure 3. Continued.

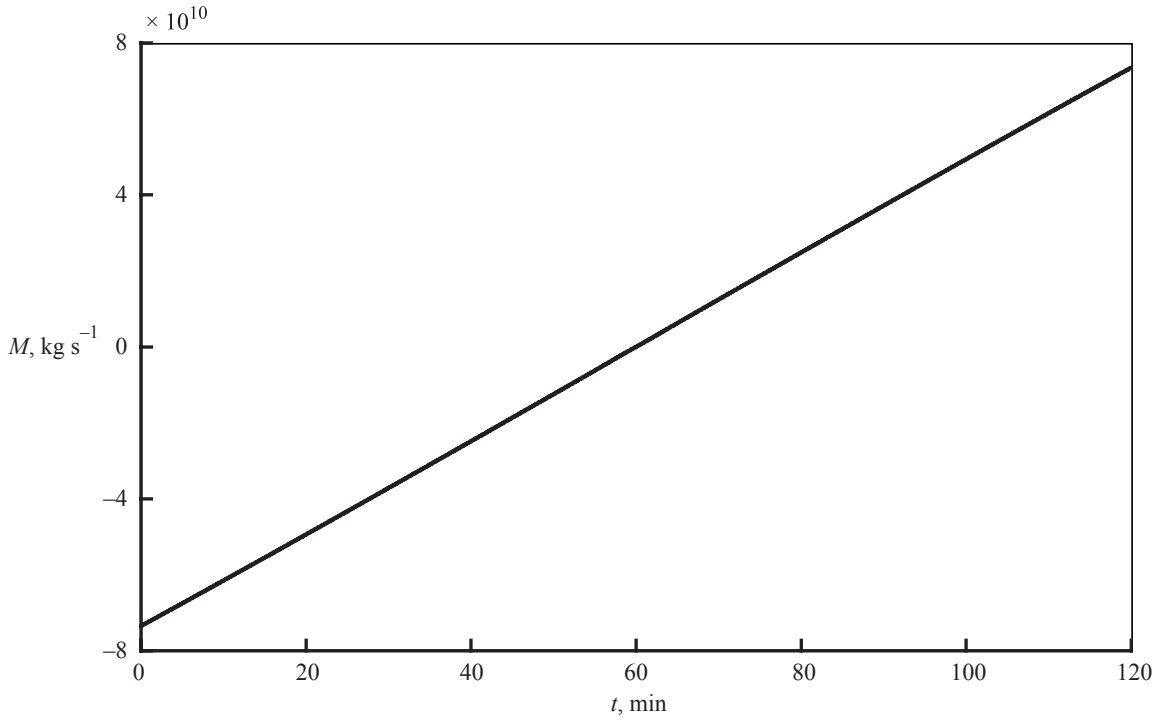

(g) Cloud base mass influx M versus t. (See eq. (4.20).)

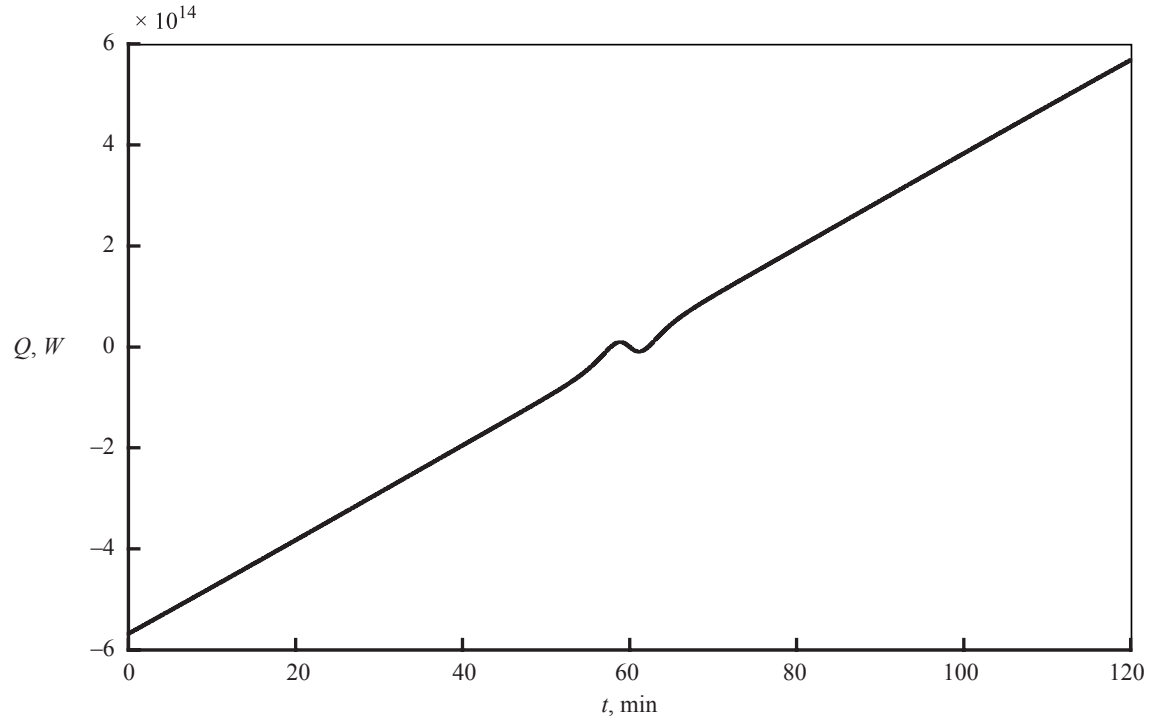

(h) Thermal input power Q versus t. (See eq. (4.26).)

Figure 3. Concluded.

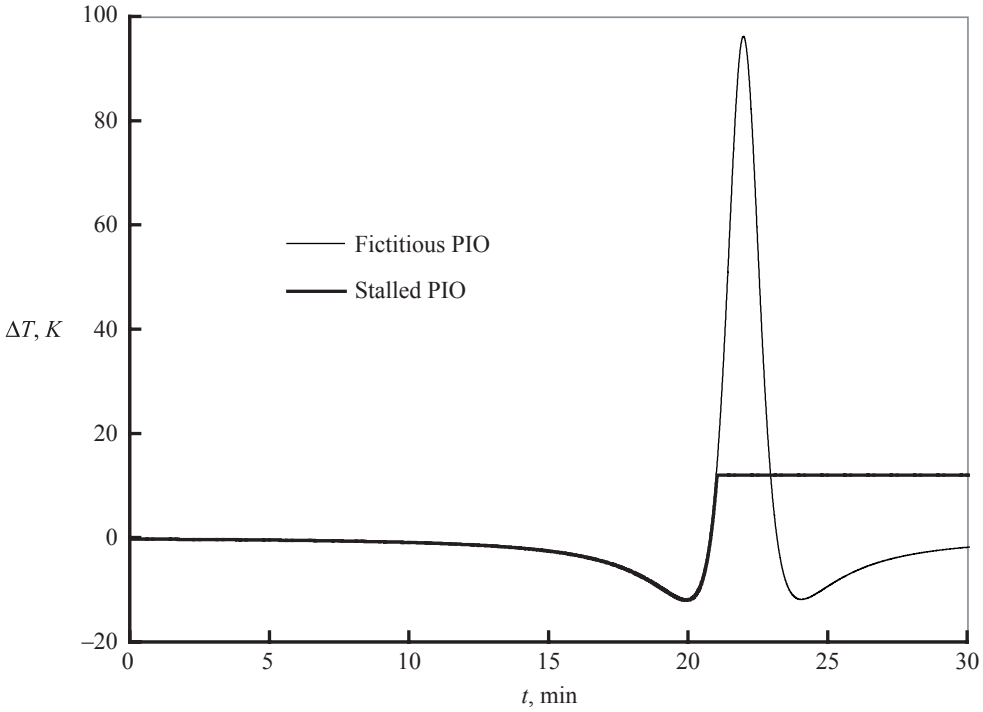

(a) Core temperature excess ΔT versus t.

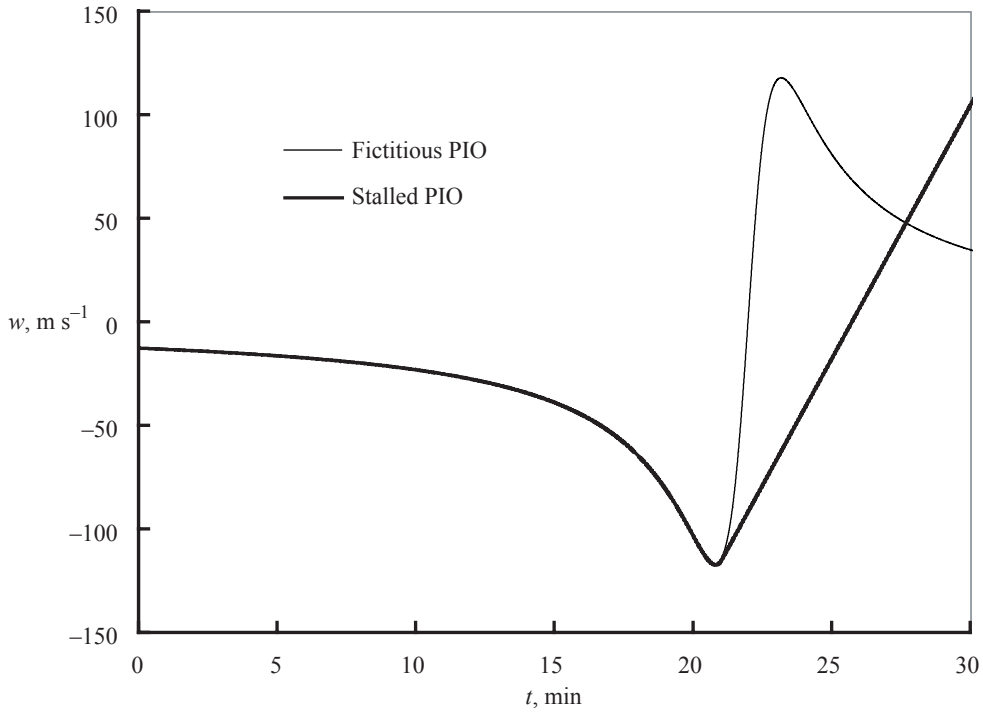

(b) Updraft speed w versus t.

Figure 4. Stalled-PIO plots for Tornadic Cyclone A9, with buoyancy B held constant after stall. Also shown for pedagogy are plots for fictitious unstalled PIO.

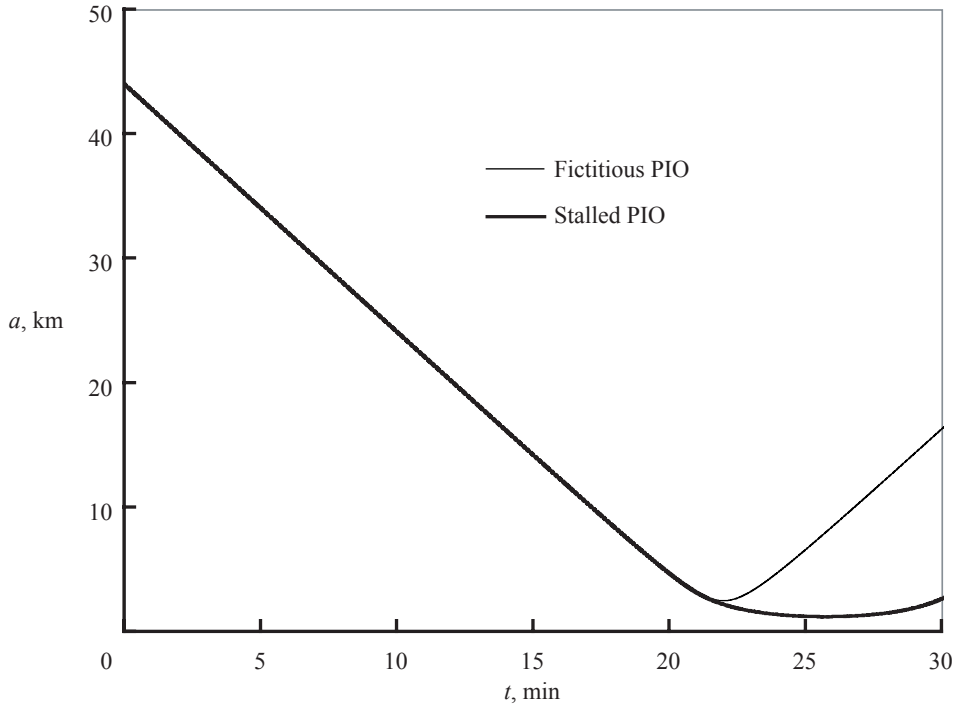

(c) Core radius a versus t.

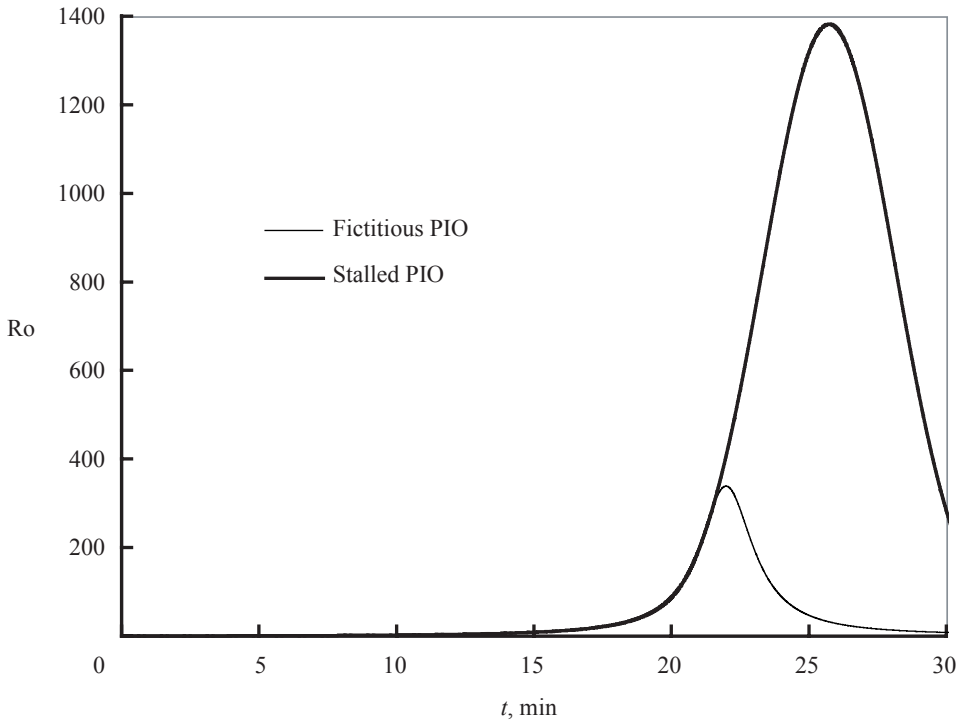

(d) Rossby number Ro versus t. (See eq. (3.2).)

Figure 4. Continued.

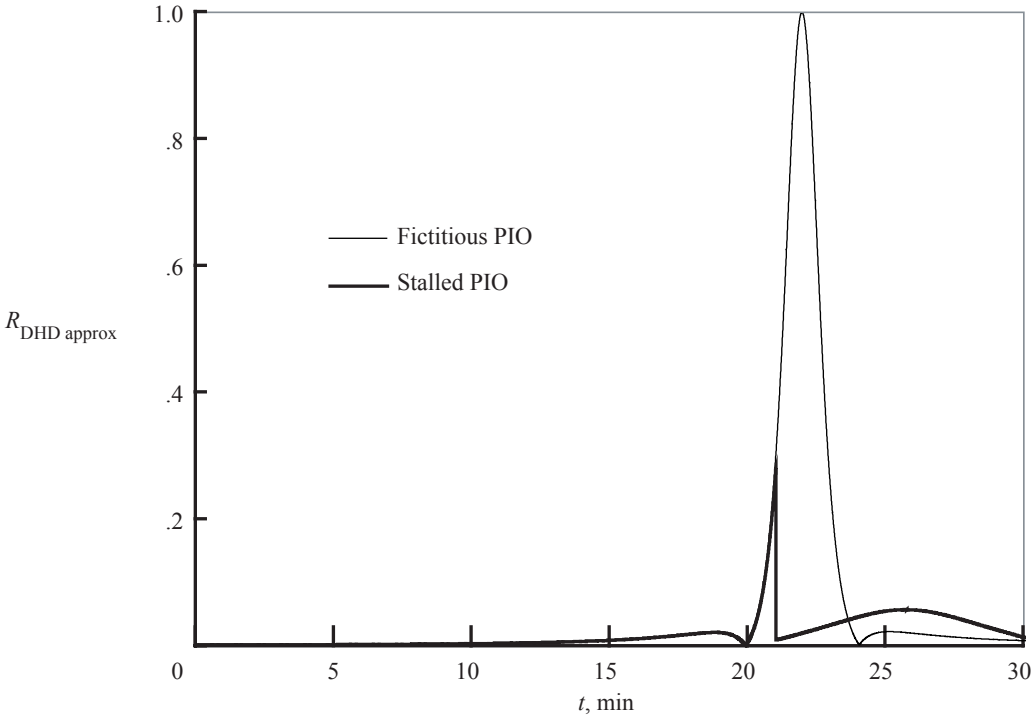

(e) Ratio $R_{\text{DHD approx}}$ of neglected terms to retained terms in DHD approximation (eq. (2.5)) versus t. (See eqs. (2.7) and (6.22).)

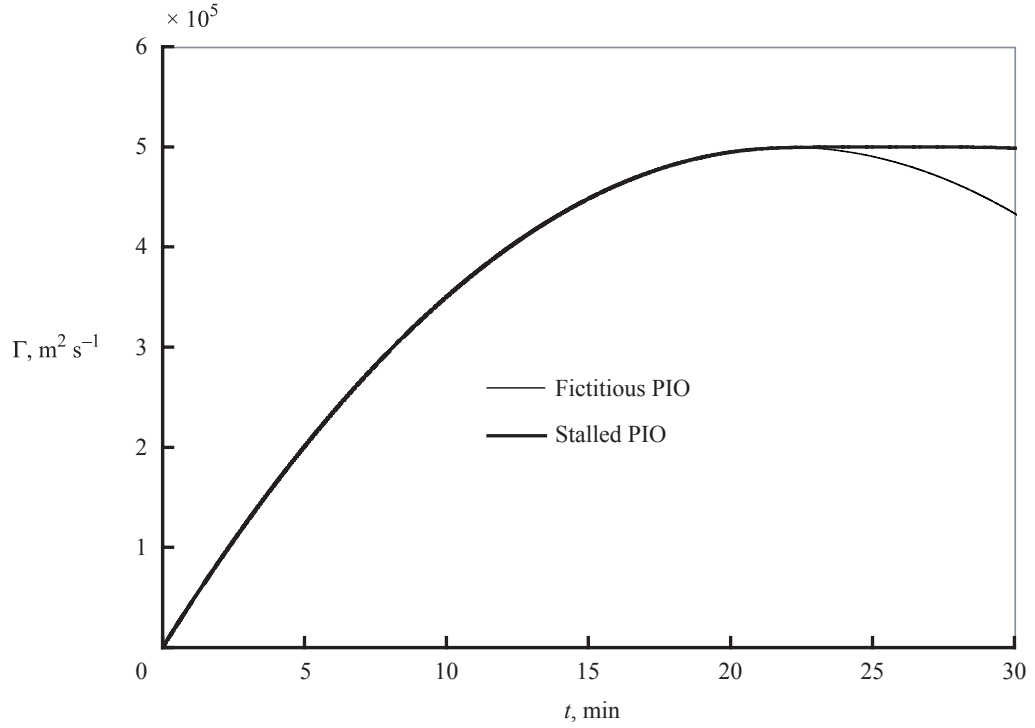

(f) Mesocyclonic circulation Γ versus t. (See eq. (4.18).)

Figure 4. Continued.

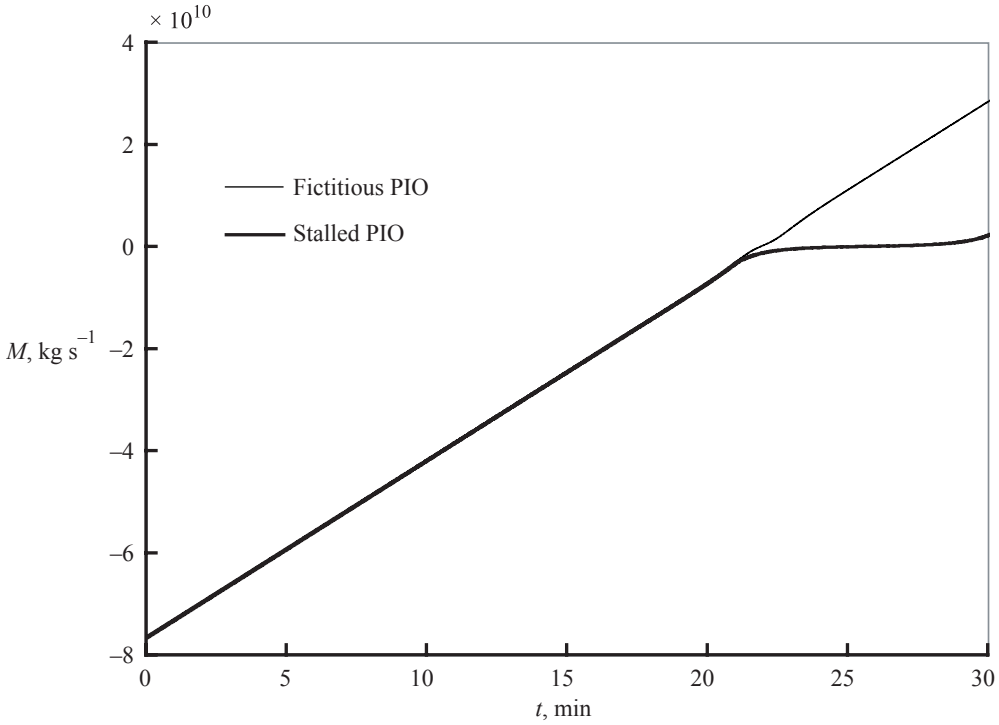

(g) Cloud base mass influx M versus t. (See eqs. (4.20) and (6.23).)

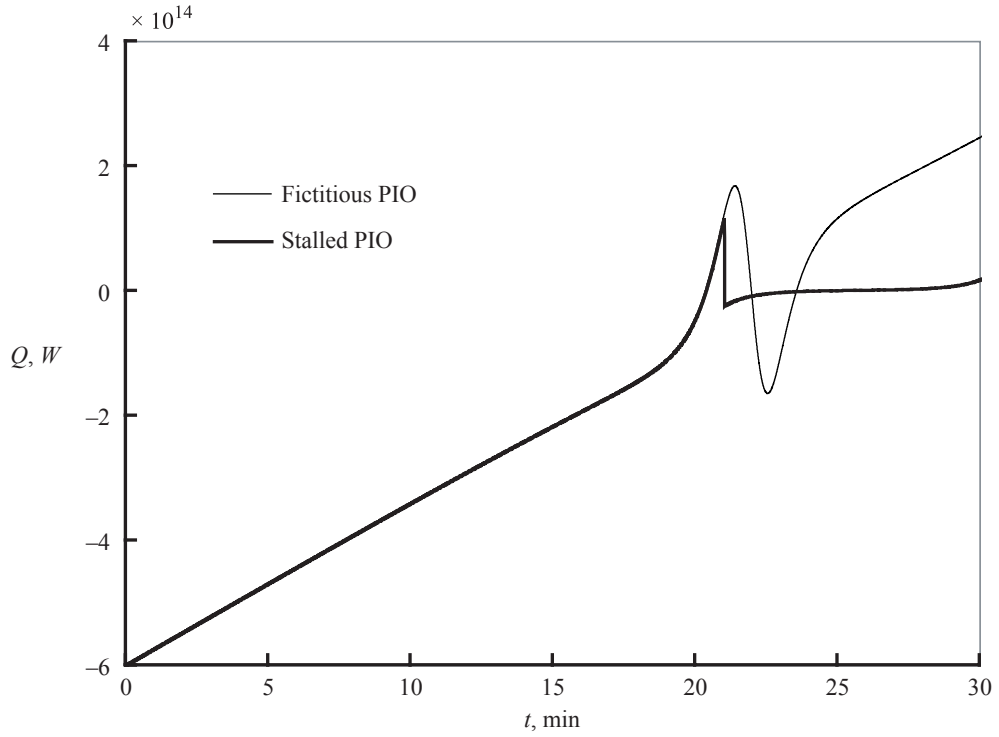

(h) Thermal input power Q versus t. (See eqs. (4.26) and (6.19).)

Figure 4. Continued.

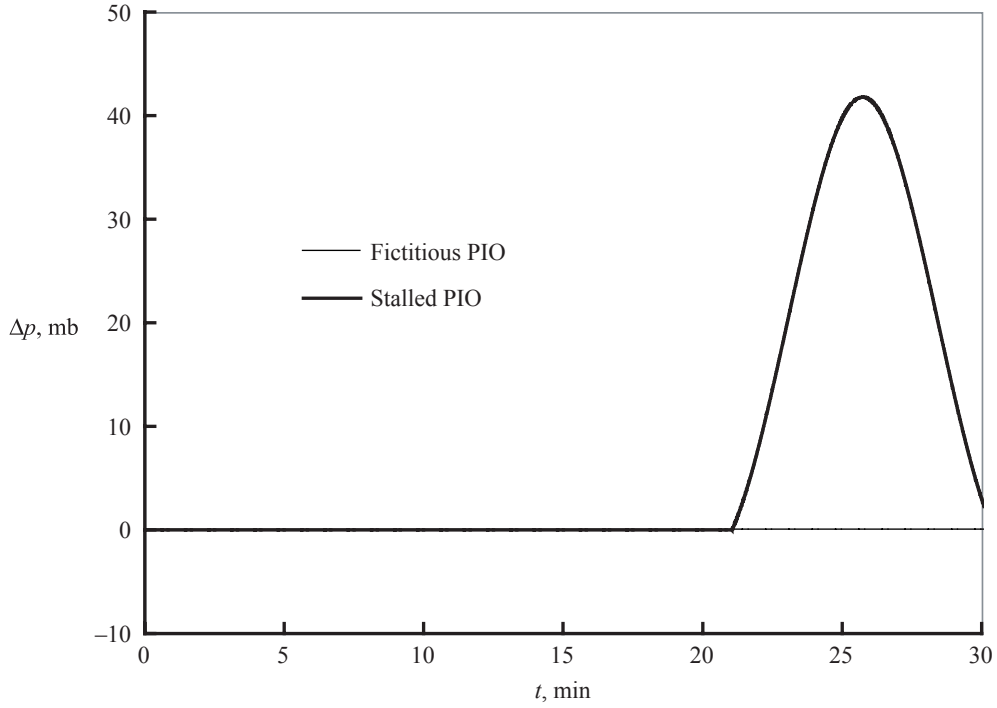

(i) Central pressure deficit Δp versus t. (See eq. (6.27).)

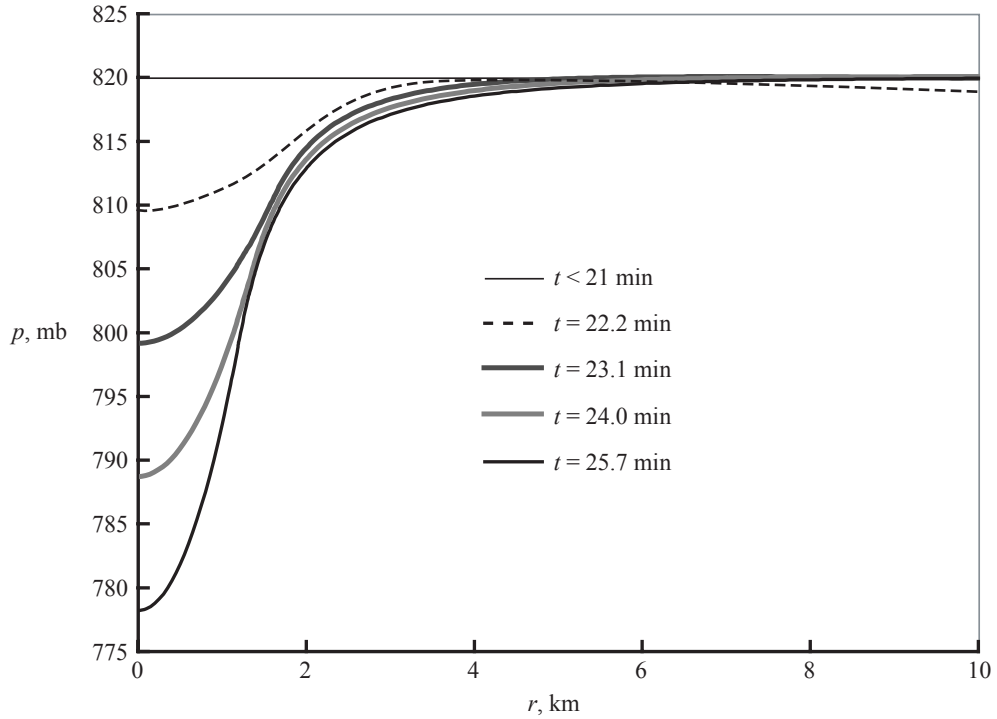

(j) Pressure p versus radius r before stall and at various times after stall. (See eqs. (6.14) and (6.16).)

Figure 4. Concluded.

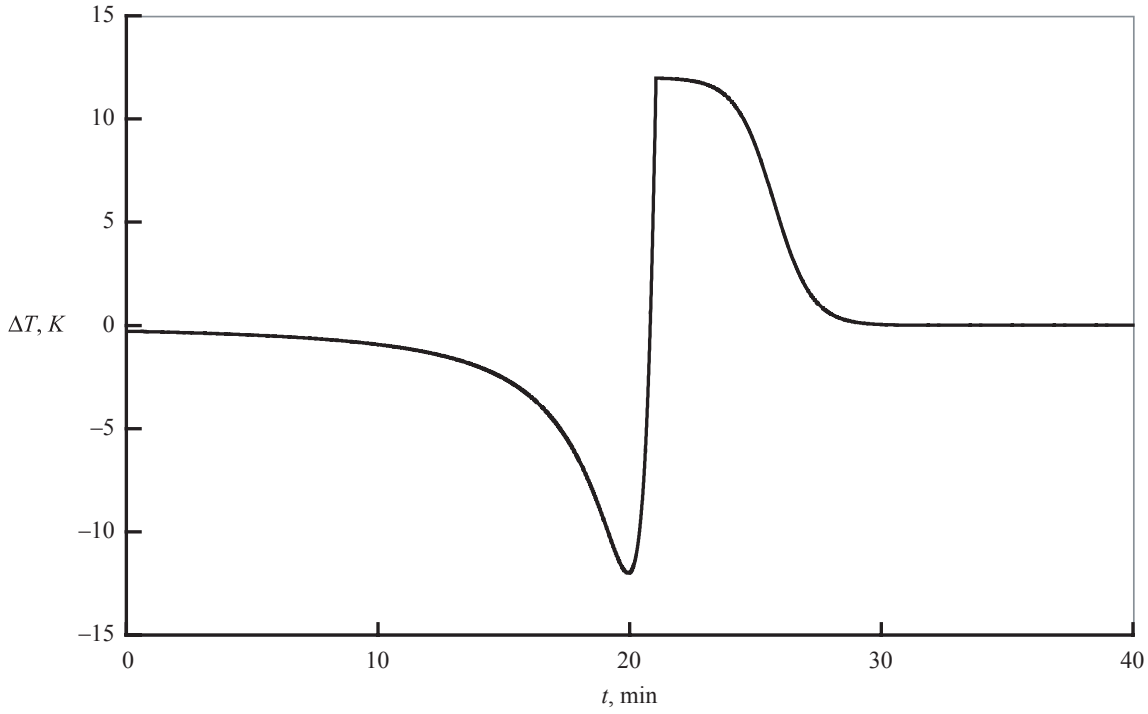

(a) Core temperature excess ΔT versus t.

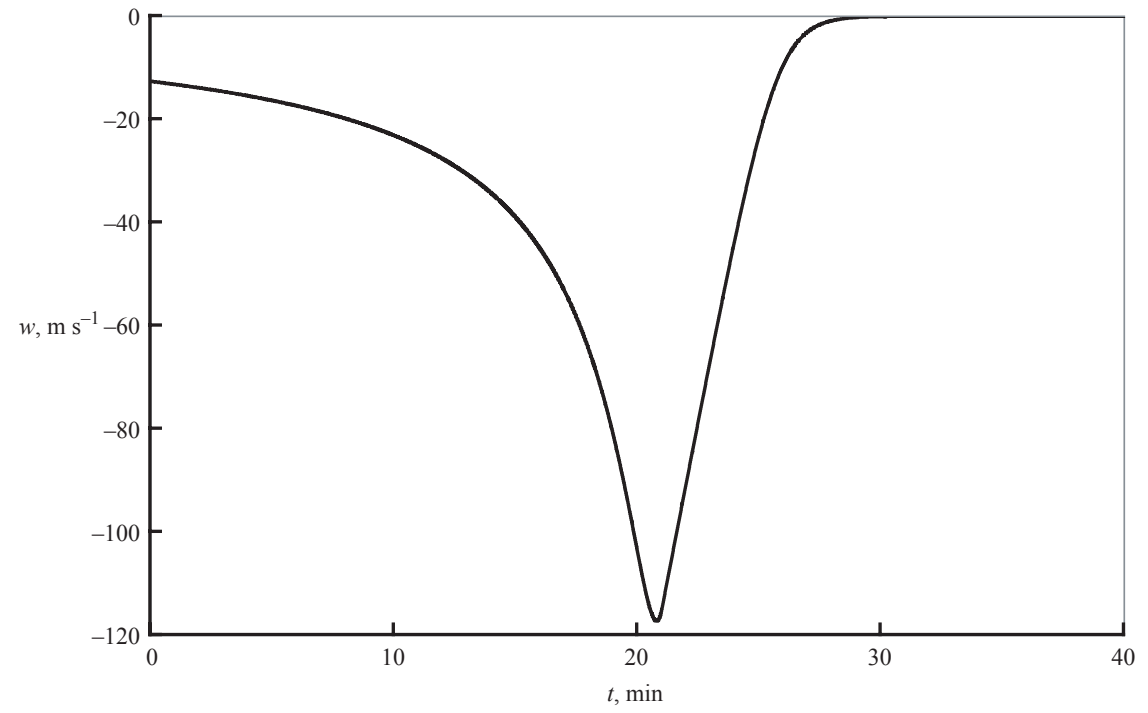

(b) Updraft speed w versus t.

Figure 5. Stalled-PIO plots for sustaining Tornadic Cyclone A9 by decreasing the buoyancy B and gradually neglecting the Coriolis force after stall.

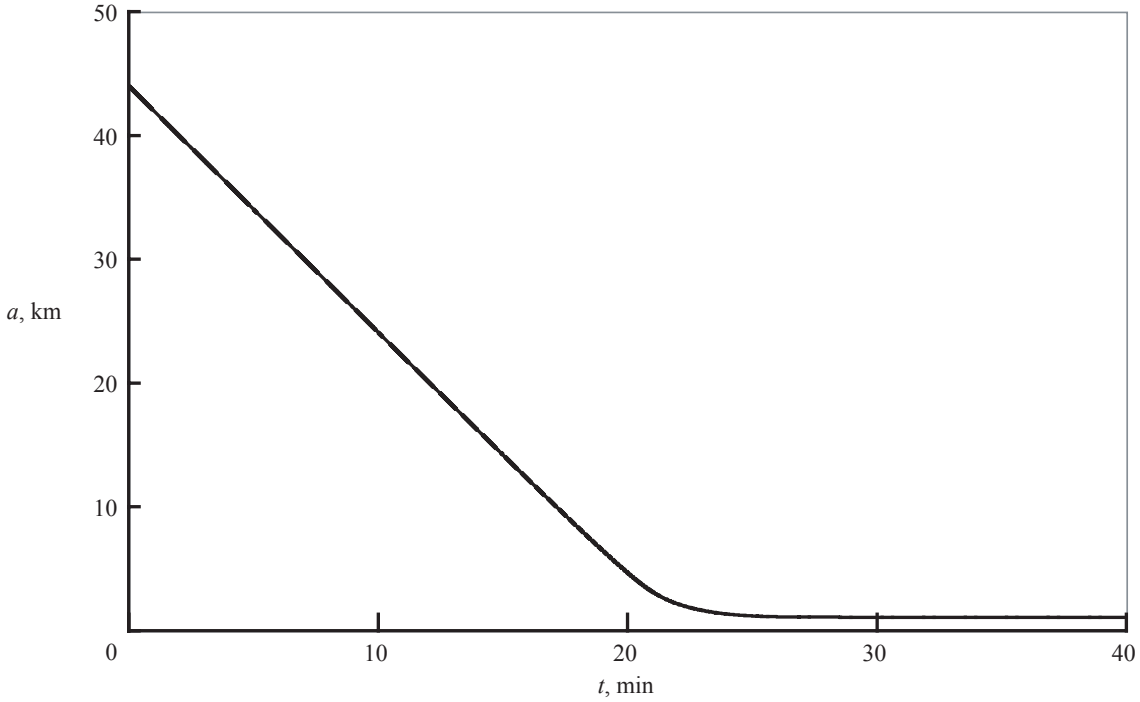

(c) Core radius a versus t.

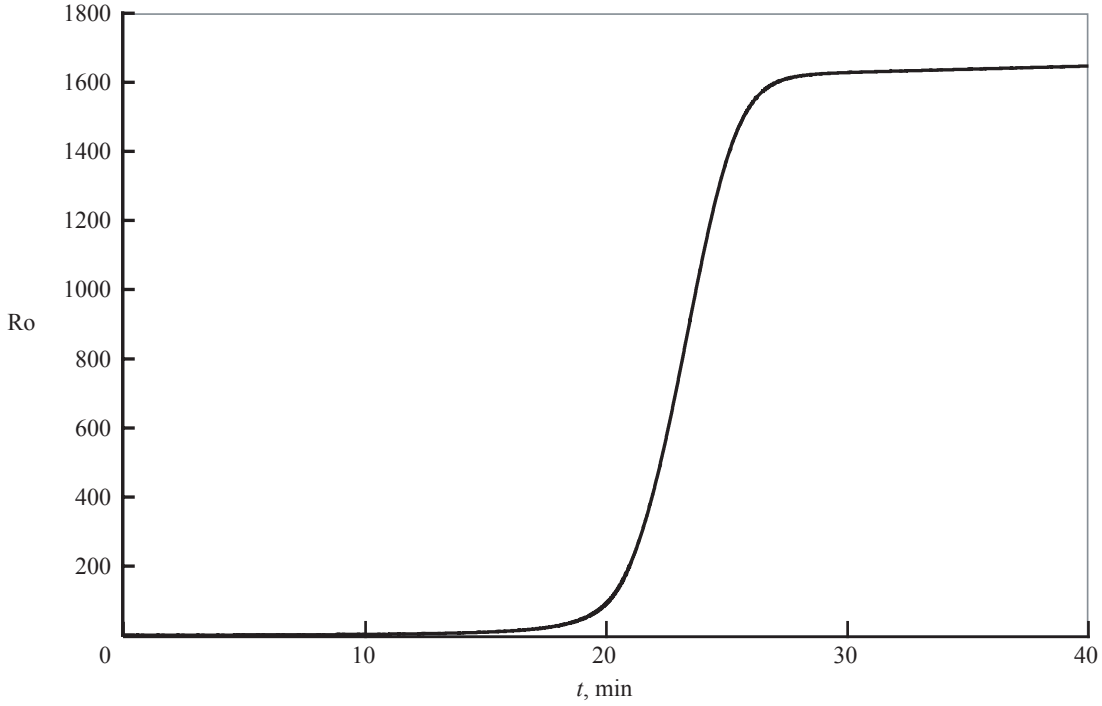

(d) Rossby number Ro versus t.

Figure 5. Continued.

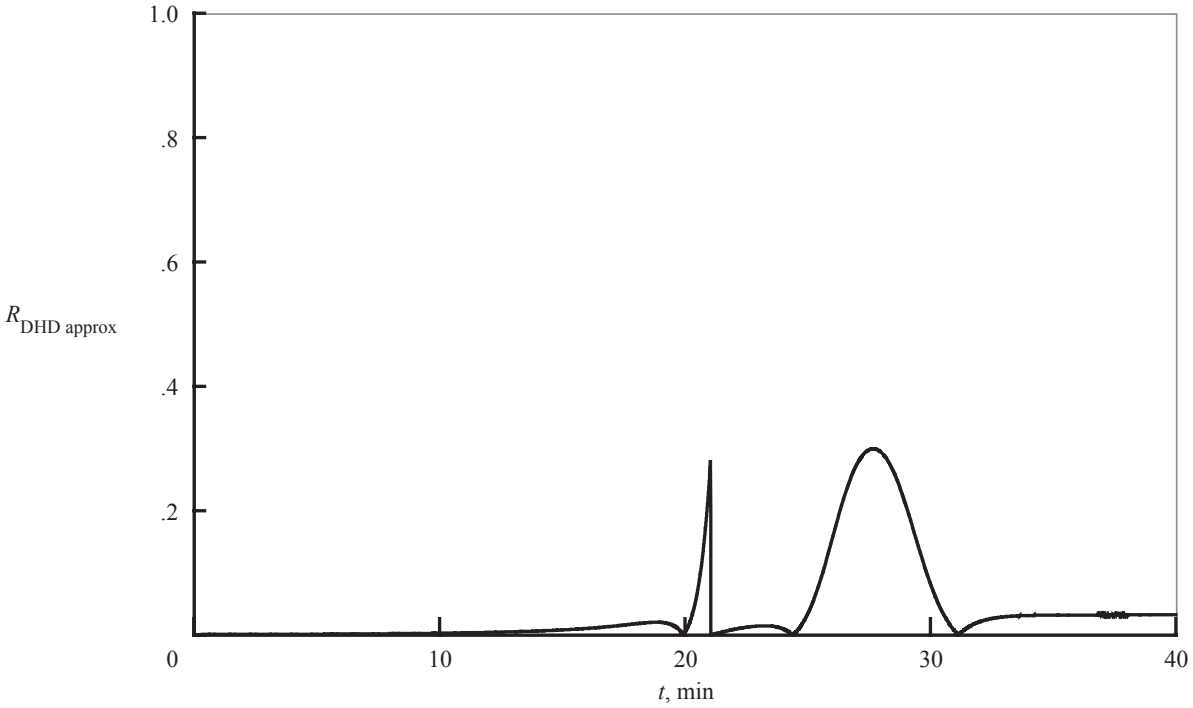

(e) Ratio $R_{\text{DHD approx}}$ of neglected terms to retained terms in DHD approximation (eq. (2.5)) versus t.

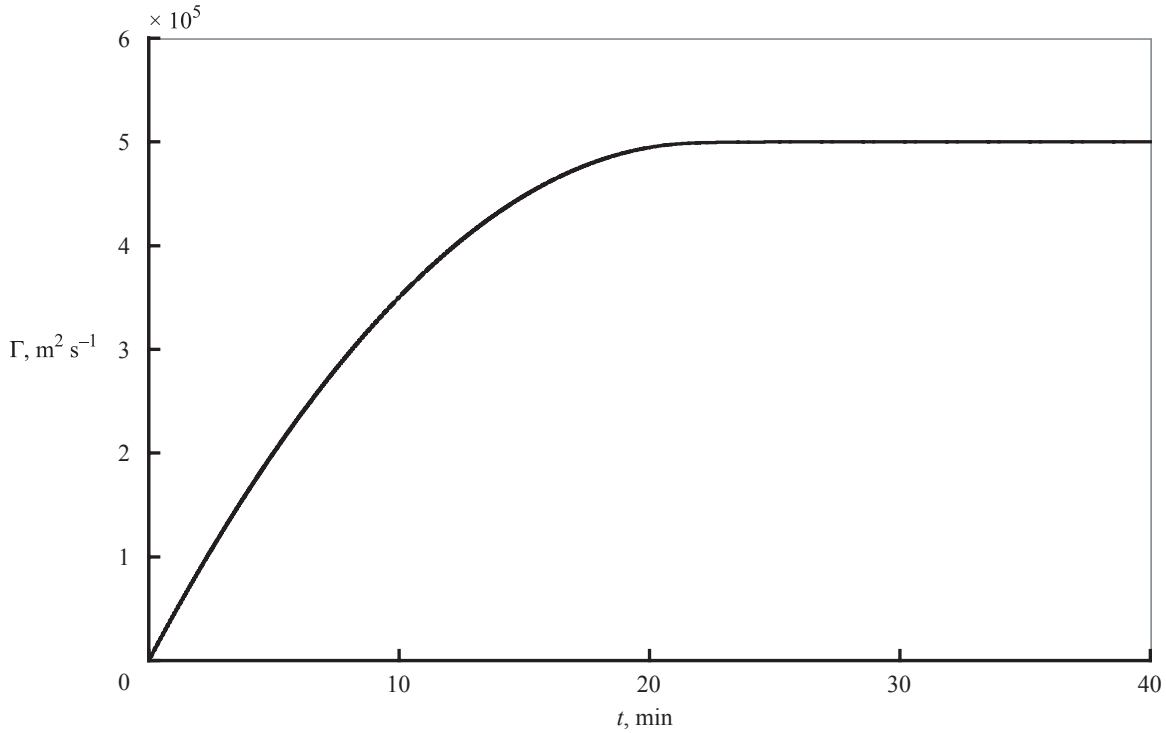

(f) Mesocyclonic circulation Γ versus t.

Figure 5. Continued.

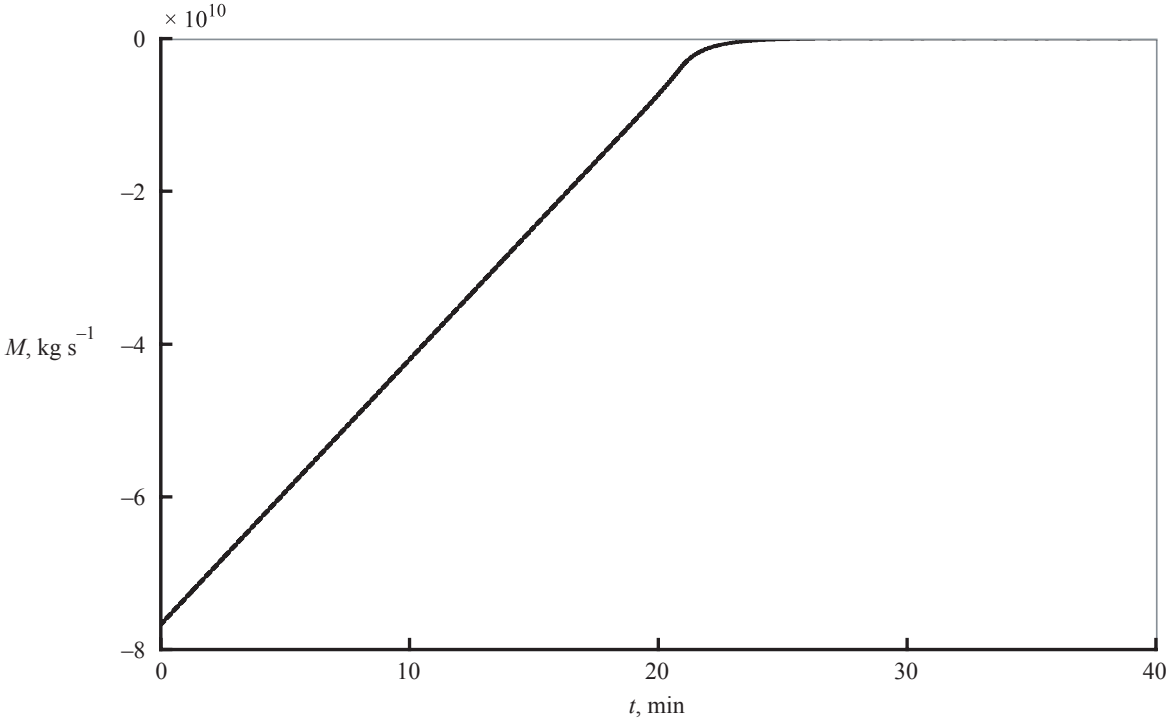

(g) Cloud base mass influx M versus t.

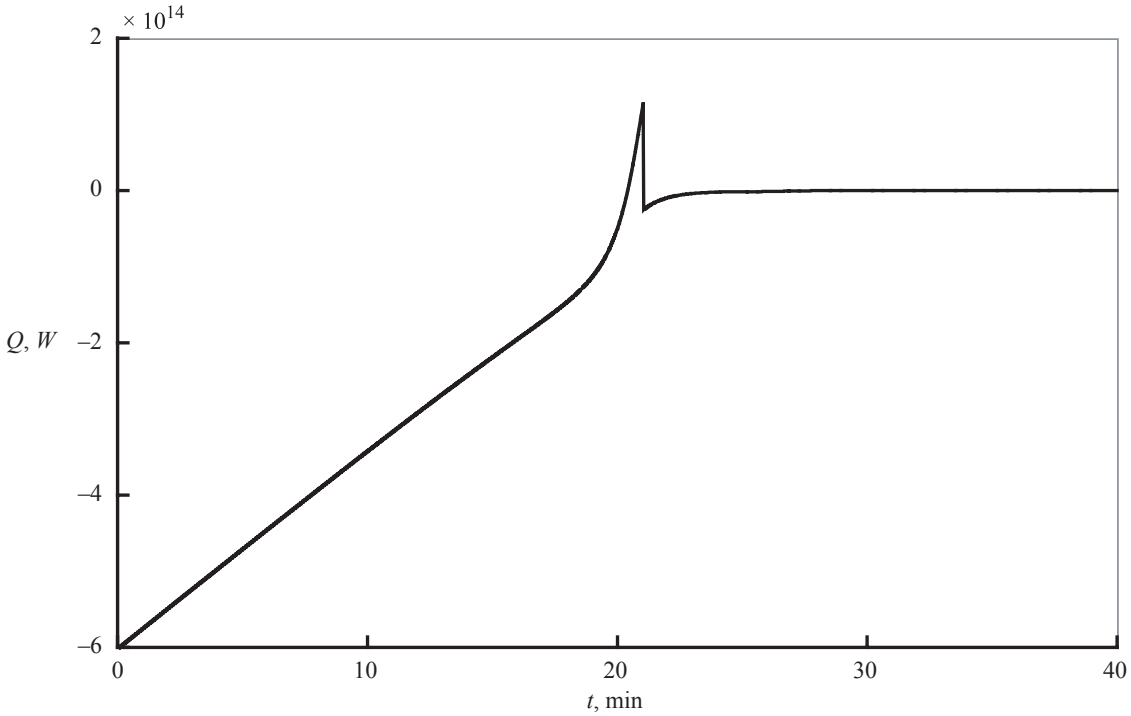

(h) Thermal input power Q versus t.

Figure 5. Continued.

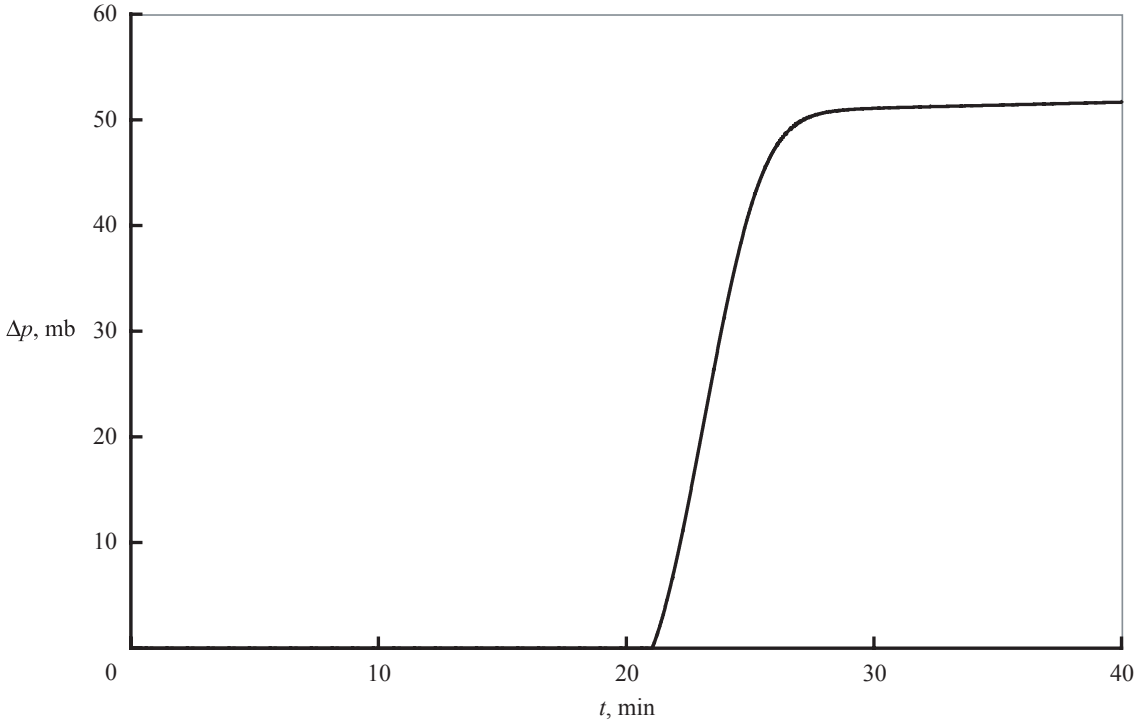

(i) Central pressure deficit Δp versus t.

Figure 5. Concluded.

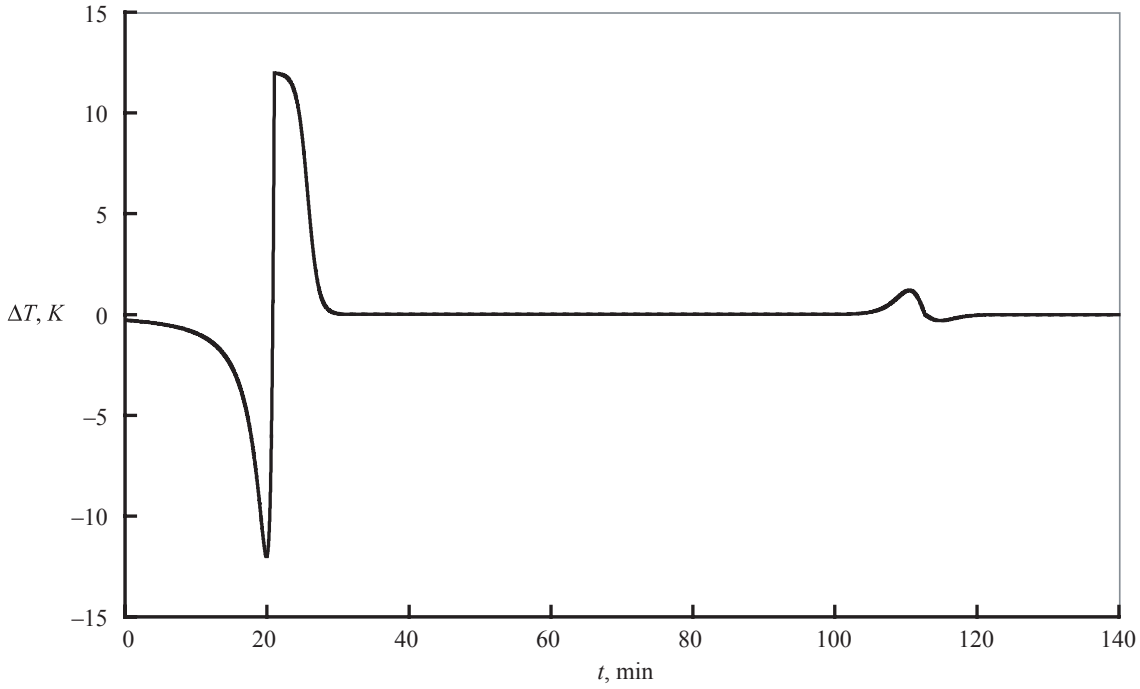

(a) Core temperature excess ΔT versus t.

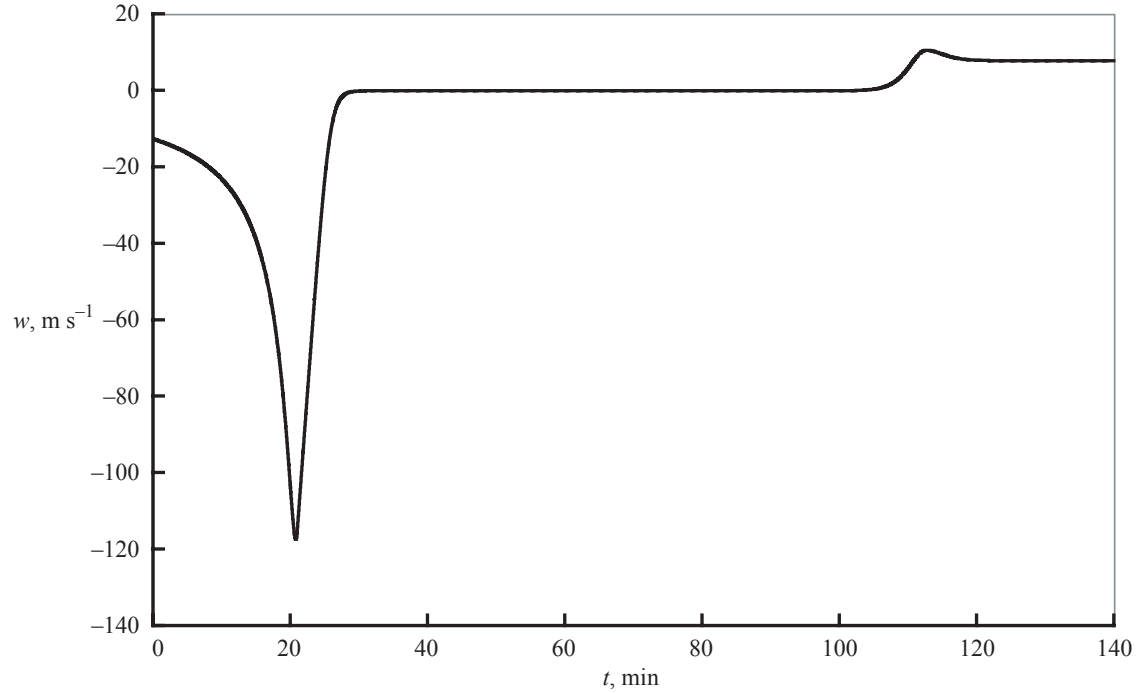

(b) Updraft speed w versus t.

Figure 6. Final stalled-PIO plots for Tornadic Cyclone A9, including its termination by further tailoring of buoyancy $B(t)$.

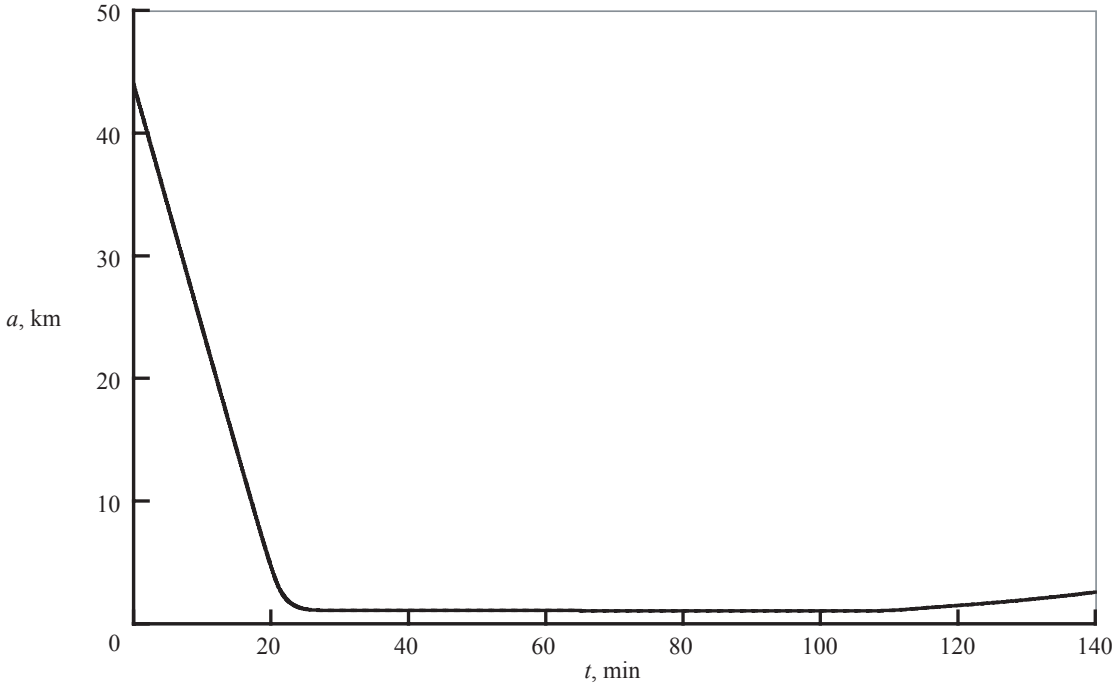

(c) Core radius a versus t.

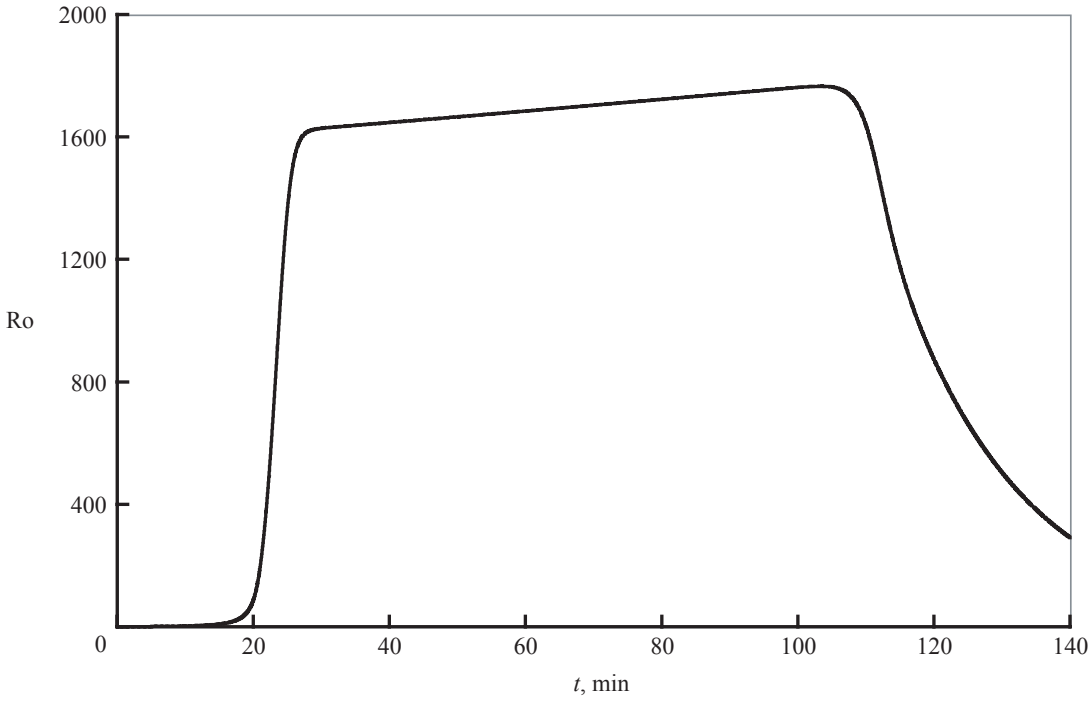

(d) Rossby number Ro versus t.

Figure 6. Continued.

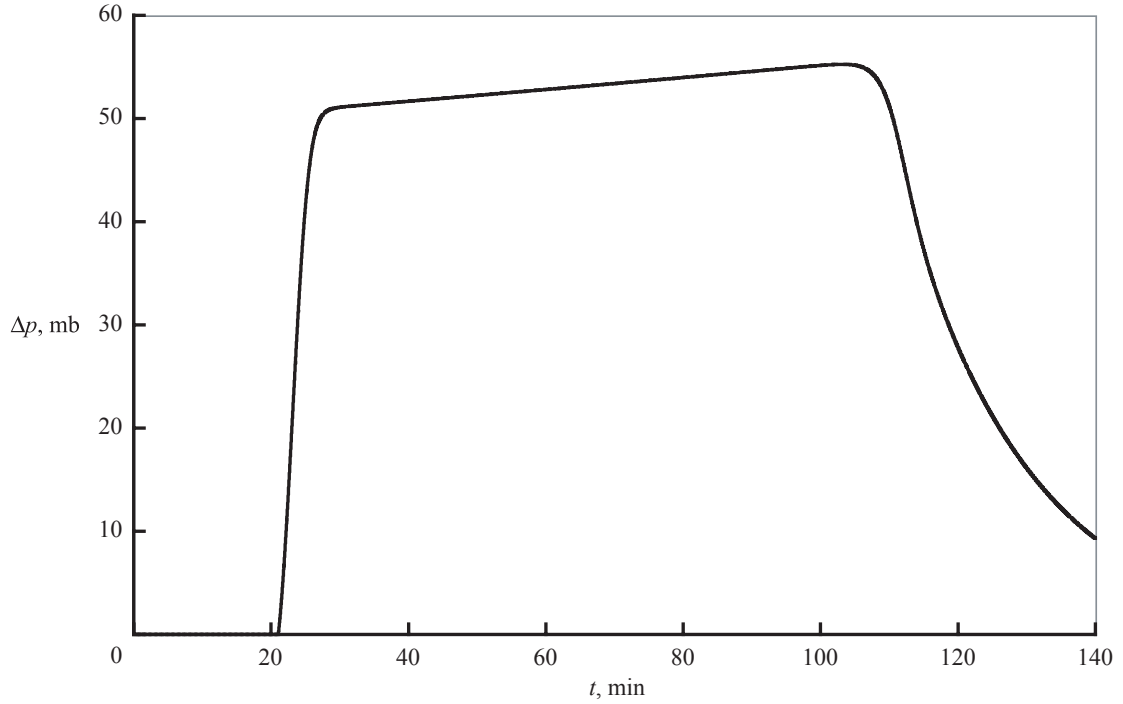

(e) Central pressure deficit Δp versus t.

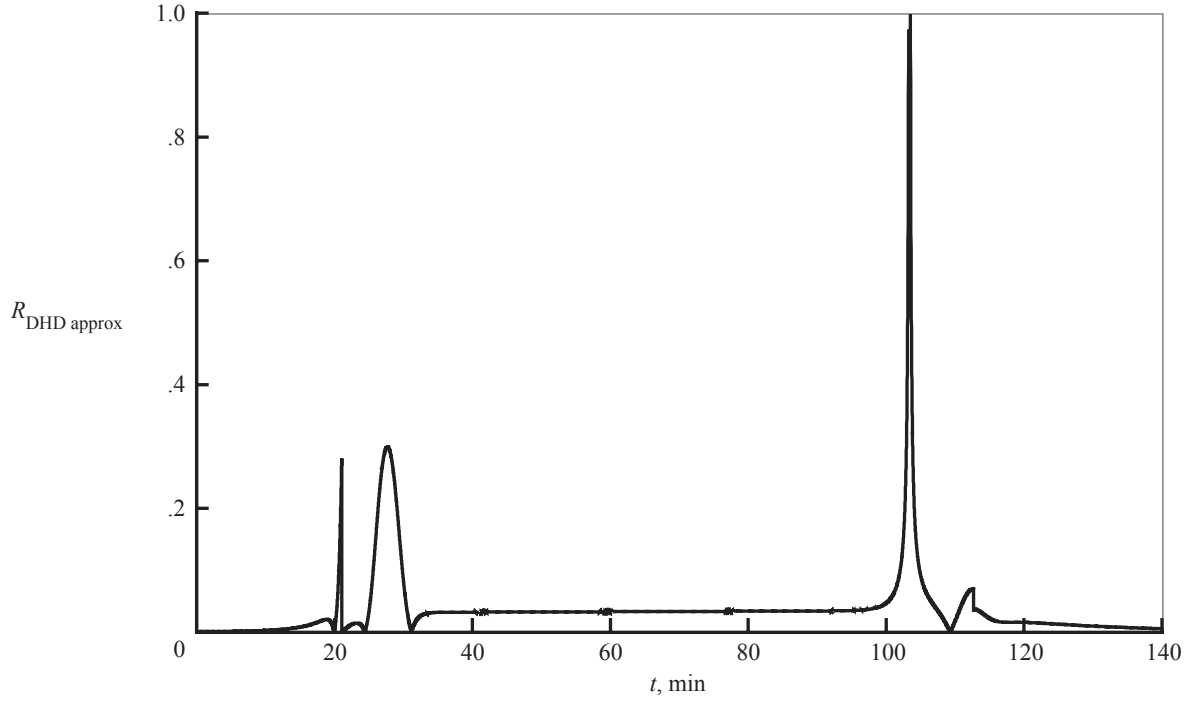

(f) Ratio $R_{\text{DHD approx}}$ of neglected terms to retained terms in DHD approximation (eq. (2.5)) versus t.

Figure 6. Continued.

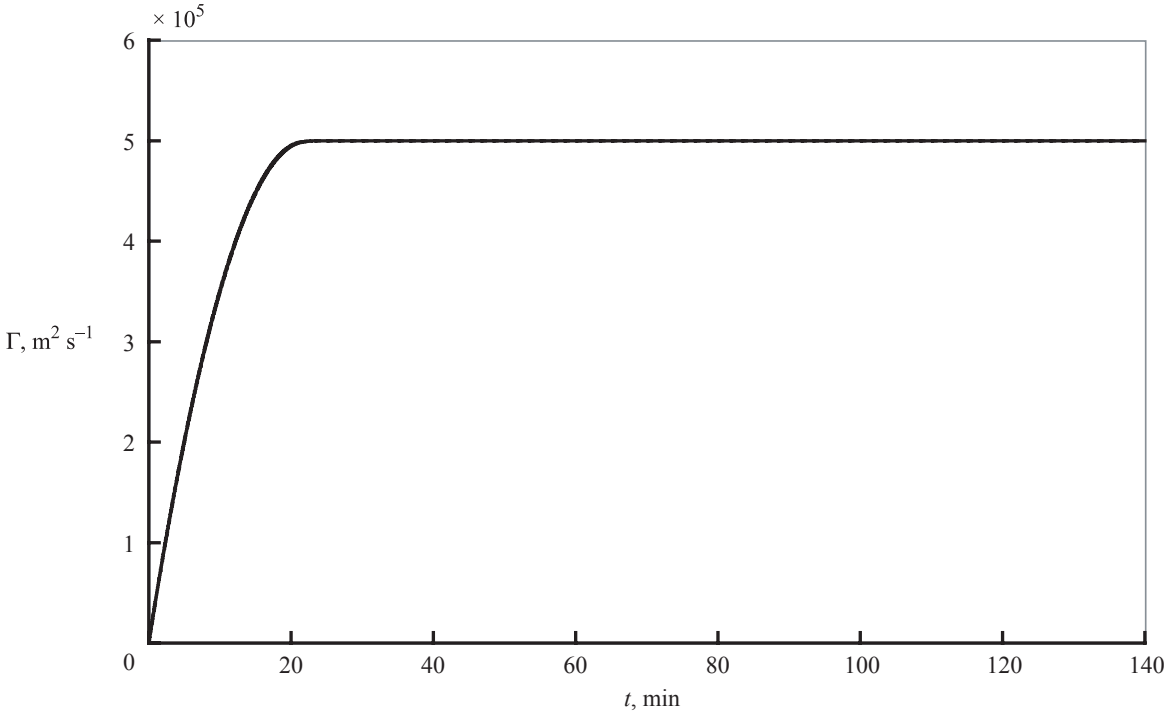

(g) Mesocyclonic circulation Γ versus t.

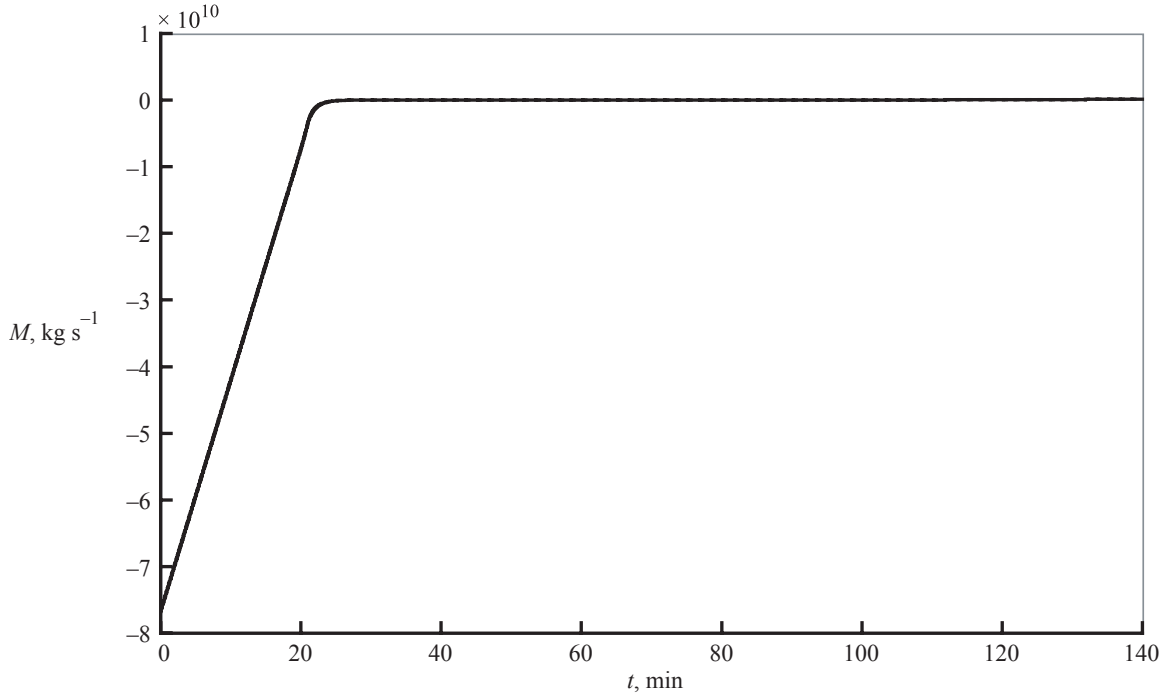

(h) Cloud base mass influx M versus t.

Figure 6. Continued.

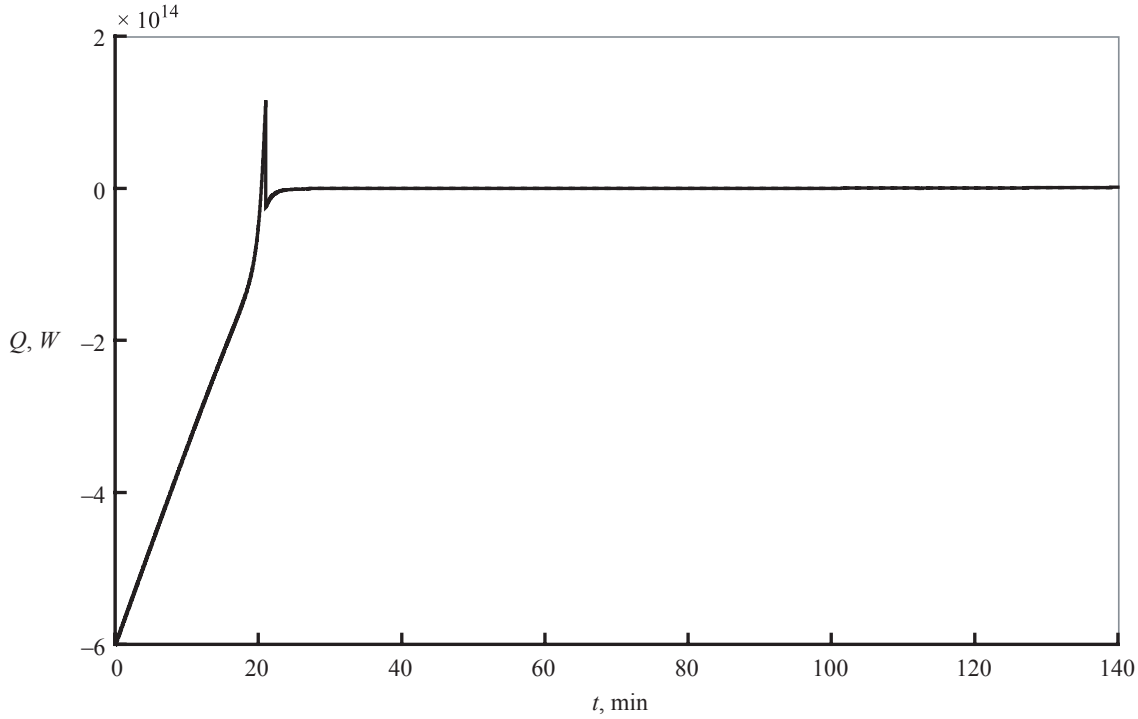

(i) Thermal input power Q versus t.

Figure 6. Concluded.

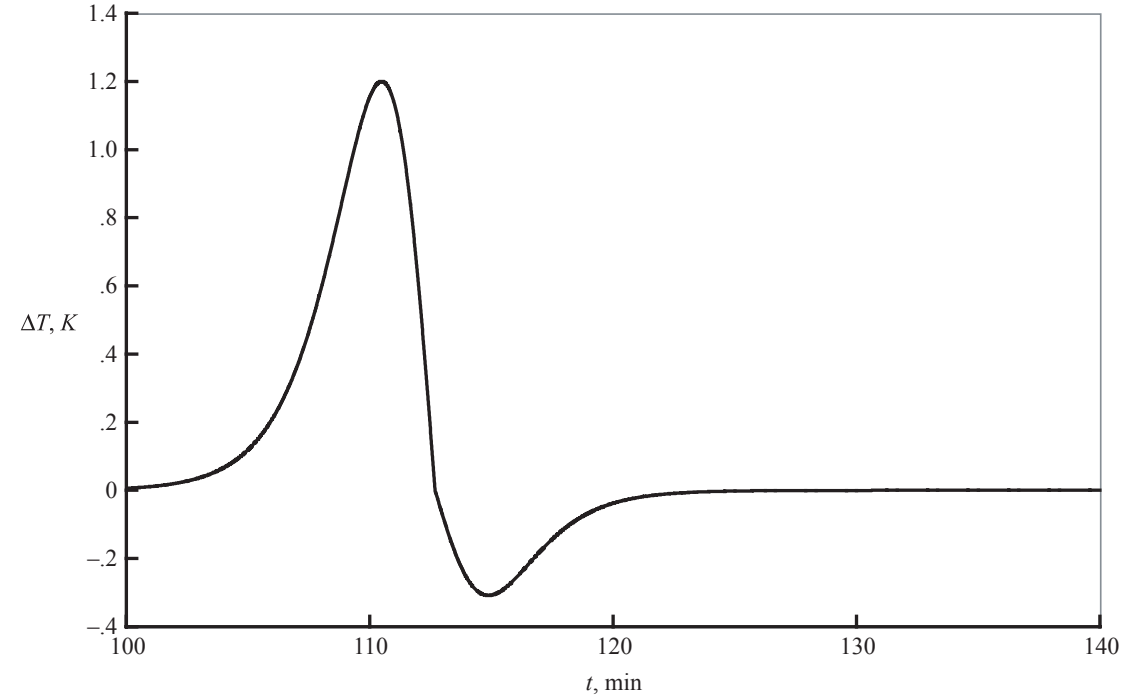

(a) Core temperature excess ΔT versus t.

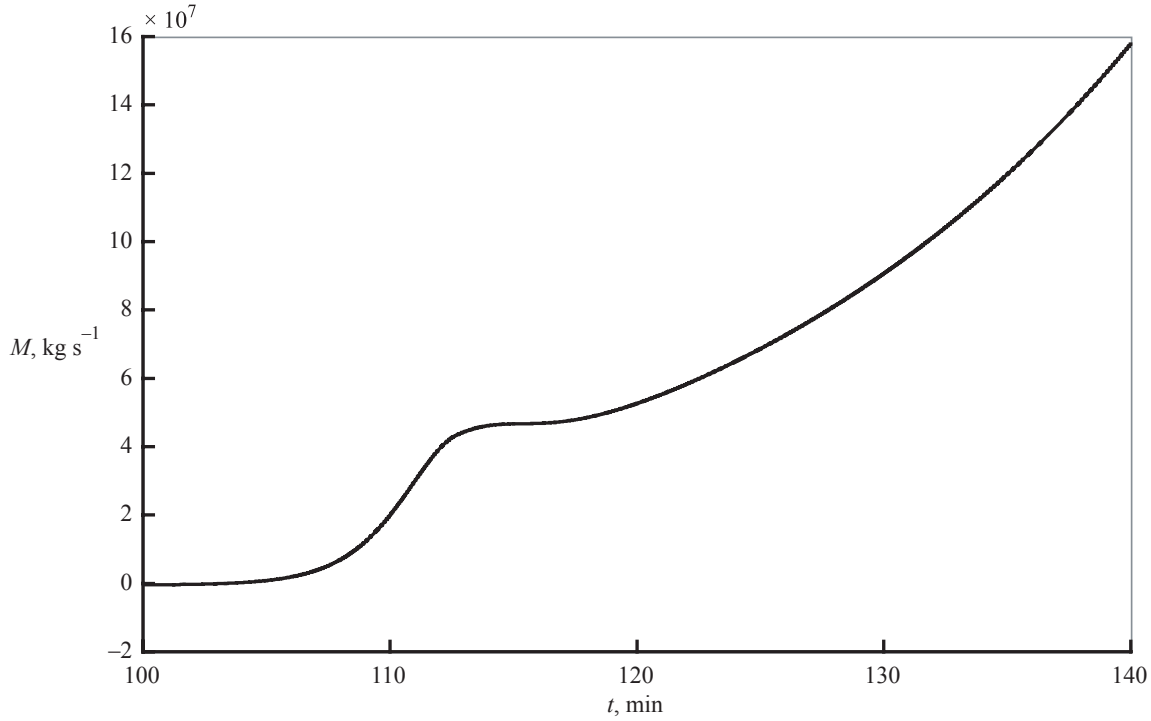

(b) Cloud base mass influx M versus t.

Figure 7. Enlarged plots of final stalled-PIO during termination phase of Tornadic Cyclone A9.

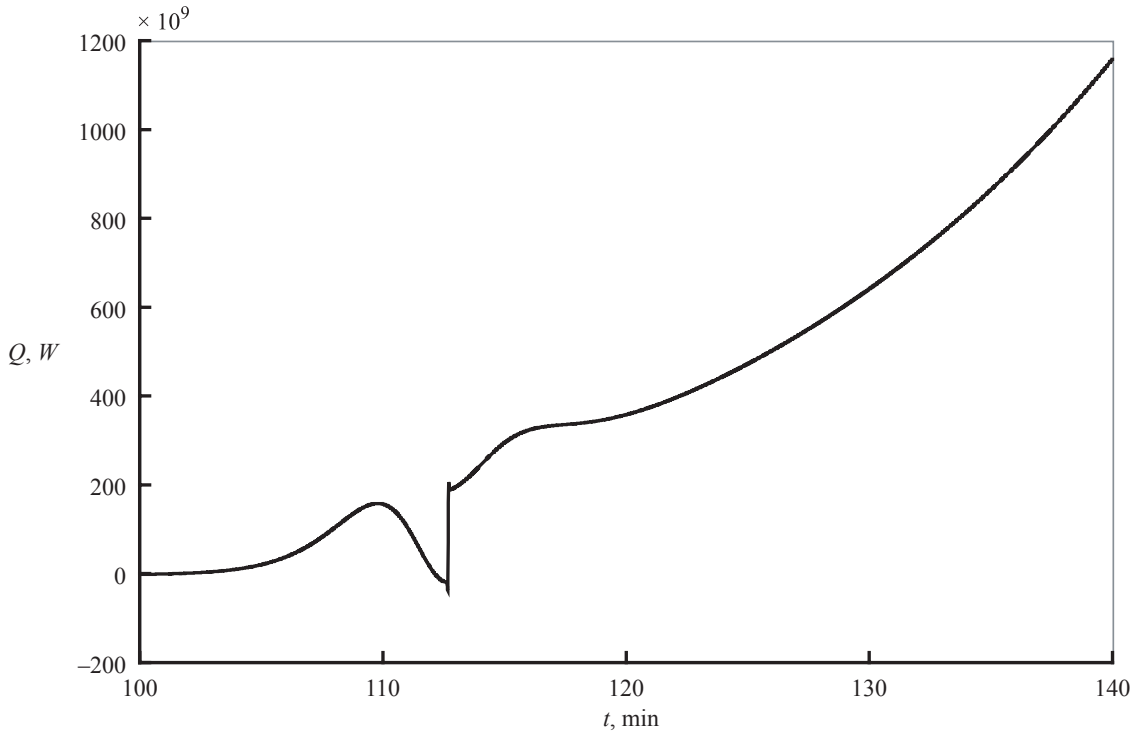

(c) Thermal input power Q versus t.

Figure 7. Concluded.

REPORT DOCUMENTATION PAGE

Form Approved
OMB No. 0704-0188

The public reporting burden for this collection of information is estimated to average 1 hour per response, including the time for reviewing instructions, searching existing data sources, gathering and maintaining the data needed, and completing and reviewing the collection of information. Send comments regarding this burden estimate or any other aspect of this collection of information, including suggestions for reducing this burden, to Department of Defense, Washington Headquarters Services, Directorate for Information Operations and Reports (0704-0188), 1215 Jefferson Davis Highway, Suite 1204, Arlington, VA 22202-4302. Respondents should be aware that notwithstanding any other provision of law, no person shall be subject to any penalty for failing to comply with a collection of information if it does not display a currently valid OMB control number.
PLEASE DO NOT RETURN YOUR FORM TO THE ABOVE ADDRESS.

1. REPORT DATE *(DD-MM-YYYY)*	2. REPORT TYPE	3. DATES COVERED *(From - To)*
01- 07 - 2005	Technical Memorandum	

4. TITLE AND SUBTITLE
Stalled Pulsing Inertial Oscillation Model for a Tornadic Cyclone

5a. CONTRACT NUMBER

5b. GRANT NUMBER

5c. PROGRAM ELEMENT NUMBER

6. AUTHOR(S)
Costen, Robert C.

5d. PROJECT NUMBER

5e. TASK NUMBER

5f. WORK UNIT NUMBER
23-762-30-51

7. PERFORMING ORGANIZATION NAME(S) AND ADDRESS(ES)
NASA Langley Research Center
Hampton, VA 23681-2199

8. PERFORMING ORGANIZATION REPORT NUMBER
L-19066

9. SPONSORING/MONITORING AGENCY NAME(S) AND ADDRESS(ES)
National Aeronautics and Space Administration
Washington, DC 20546-0001

10. SPONSOR/MONITOR'S ACRONYM(S)
NASA

11. SPONSOR/MONITOR'S REPORT NUMBER(S)
NASA/TM-2005-213514

12. DISTRIBUTION/AVAILABILITY STATEMENT
Unclassified - Unlimited
Subject Category 47
Availability: NASA CASI (301) 621-0390

13. SUPPLEMENTARY NOTES
Costen, Langley Research Center, Hampton, VA.
An electronic version can be found at http://ntrs.nasa.gov

14. ABSTRACT

A supercell storm is a tall, rotating thunderstorm that can generate hail and tornadoes. Two models exist for the development of the storm's rotation or mesocyclone—the conventional splitting-storm model, and the more recent pulsing inertial oscillation (PIO) model, in which a nonlinear pulse represents the supercell. Although data support both models and both could operate in the same supercell, neither model has satisfactorily explained the tornadic cyclone. A tornadic cyclone is an elevated vorticity concentration of Rossby number approximately 1000 that develops within the contracting mesocyclone shortly before a major tornado appears at the surface. We now show that if the internal temperature excess due to latent energy release is limited to the realistic range of –12 K to +12 K, the PIO model can stall part way through the pulse in a state of contraction and spin-up. Should this happen, the stalled-PIO model can evolve into a tornadic cyclone with a central pressure deficit that exceeds 40 mb, which is greater than the largest measured value. This simulation uses data from a major tornadic supercell that occurred over Oklahoma City, Oklahoma, USA, on May 3, 1999. The stalled-PIO mechanism also provides a strategy for human intervention to retard or reverse the development of a tornadic cyclone and its pendant tornado.

15. SUBJECT TERMS
Tornadic cyclone; Stalled pulsing inertial oscillation model; Dilatation-horizontal divergence approximation; Oklahoma City tornado, May 3, 1999; Strategy for human intervention

16. SECURITY CLASSIFICATION OF:			17. LIMITATION OF ABSTRACT	18. NUMBER OF PAGES	19a. NAME OF RESPONSIBLE PERSON
a. REPORT	b. ABSTRACT	c. THIS PAGE			STI Help Desk (email: help@sti.nasa.gov)
					19b. TELEPHONE NUMBER *(Include area code)*
U	U	U	UU	56	(301) 621-0390